Ludwig-Maximillians-Universtät Müchen
Technische Universität Müchen
Max-Planck-Institut Für Quantumoptik


# Spectral Analysis of Quantum Many Body Systems with Tensor Network Algorithms

München 2021 Yilun Yang （杨逸伦）

# Spectral Analysis of Quantum Many Body Systems with Tensor Network Algorithms

**Yilun Yang** （杨逸伦）

Thesis submitted
within the Elite Master Program
Theoretical and Mathematical Physics
of Ludwig–Maximilians–Universität
München

Supervised by:
Prof. Dr. Ignacio Cirac
Dr. Dr. Mari Carmen Bañuls

München, submitted upon completion

# Abstract

It has been a long time open question how a closed quantum mechanical system thermalizes. The difficulty lies in simulating sufficiently long time evolutions of quantum many-body Hamiltonians within controllable errors. In this work, we present a method to probe thermalization by instead exploring spectral properties, which goes well beyond what direct time-dependent simulations have been able to achieve so far (Yang et al., 2020). We combine tensor network techniques with Chebyshev polynomial expansions to compute a class of generalized density of states, through which the long time average of given initial states and microcanonical ensemble expectations can be obtained. They allow probes of initial state thermalization as well as the weak eigenstate thermalization hypothesis. The Ising and PXP spin chains are illustrated as examples, where our results are in line with the expectations from theory and numerics in small size systems.

# Contents

# List of Figures

# Chapter 1

# Introduction

Quantum mechanics has profoundly changed people's understanding of physics since its emergence in the last century. The key result is that the dynamics in the microscopic world is governed by the Schrödinger's equation. Despite the seemingly simple form, the Schrödinger's equation becomes extremely complicated when applied to many body systems. A standard quantum mechanical approach is to treat the interactions as perturbations of strength $\lambda$ to the non-interacting Hamiltonian and expand the physical quantities in a power series of $\lambda$. Nevertheless it fails in strongly-correlated systems and the Hamiltonian has to be considered as a whole.

Effective lattice models are often adopted, which encode essential information of the full Hamiltonian (*i.e.*, low-lying excitations) with finite local dimensions. The total Hilbert space dimension, however, still grows exponentially with the system size. For a spin-1/2 chain with 100 sites, the Hilbert space dimension is $2^{100} \approx 1.27 \times 10^{30}$, far beyond the reach of any classical computer.

There are multiple ways to avoid such exponential walls. One powerful method is quantum Monte Carlo (QMC) (Foulkes et al., 2001; Gull et al., 2011) that stochastically samples the required density operators. QMC can be efficiently applied to large systems with hundreds of sites, but it suffers from the sign problem in most fermionic and frustrated spin systems (Troyer and Wiese, 2005), which destroys the efficiency.

The tensor networks (TN) (Cirac et al., 2020; Schollwöck, 2011), as an alternative, tackle the drawback of QMC. They are variational ansätze that use polynomial number of coefficients in system size to represent states and operators satisfying the so-called area laws of entanglement (Eisert et al.,

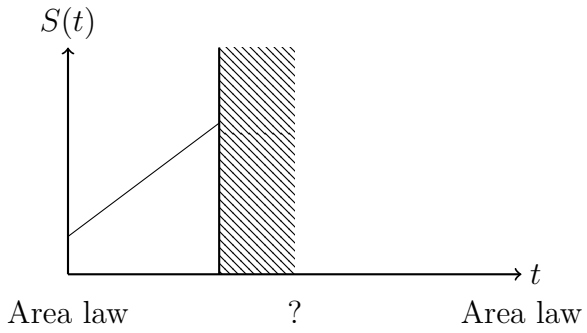


Figure 1.1: Growth of the entanglement entropy $S(t)$ of a quenched product state.

2010). Area laws are common properties among many states of physical interests, including ground (Hastings, 2007) and thermal states (Wolf et al., 2008) of local Hamiltonians, for which algorithms based on one-dimensional TN, namely matrix product states (MPS) and matrix product operators (MPO), are highly successful.

When talking about the mechanisms of quantum thermalization, states and operators beyond area laws will however be involved. With discussions dated back to 1920s (Deutsch, 2018), it is still not yet clear in general how to enter quantum equilibrium from microscopic structures. Given an initial one-dimensional many-body product state that can be efficiently represented by an MPS, its entanglement entropy can grow linearly with regard to evolving time (Calabrese and Cardy, 2005) and soon exceed the representating ability of MPS. While its long time average, as a density matrix, could be well approximated by an MPO in the case of thermalization. It is yet not clear how to switch between these two regimes.

Other than the evolution of initial states, thermalization can also be understood on the level of energy eigenstates. The eigenstate thermalization hypothesis (ETH) (Deutsch, 1991; Srednicki, 1994) proposes that physically relevant local observables are close to a smooth function of energy when evaluated for each energy eigenstate. One has to go to highly-excited energy eigenstates at finite temperatures in order to directly check the validity of ETH. If these states encode the local properties of the thermal systems (Kaufman et al., 2016; Popescu et al., 2006), they will follow volume laws with extensive entanglement and are out of reach by TN techniques.

There have been a few TN algorithms (Enss and Sirker, 2012; Hartmann

et al., 2009; Kim et al., 2015) trying to avoid the explicit representation of such states. Although they extend the applicability of the toolbox and allow access to additional dynamical quantities in some scenarios, the fundamental goal of accessing the long time behavior in a general case, and thus deciding the appearance of equilibration or thermalization, has not been achieved.

In this thesis, we introduce a new powerful method to fill in these gaps (Yang et al., 2020). It is based on a family of generalized density of states (GDOS)

$$g(E, \hat{O}) = \mathrm{tr}\left[\hat{O}\delta(E - \hat{H})\right]. \tag{1.1}$$

The $\delta$ operators, serving as filters of narrow energy intervals, can be expanded in terms polynomials of the Hamiltonian $\hat{H}$ by the kernel polynomial method (Weiße et al., 2006), such that the GDOS can be approximated with MPS and MPO. This scheme provides access not only to the full density of states (DOS, by setting $\hat{O} = \mathbb{1}$), but also to energy functions intimately related to out-of-equilibrium dynamics including the local density of states (LDOS, by setting $\hat{O} = |\psi\rangle\langle\psi|$ a projector onto a pure state). It offers the probability to probe ETH across the spectrum and to reach long time average of initial states without explicitly simulating the time evolution.

**Organization of this thesis.**

In Chapter 2, an overview of background knowledge is given from two aspects. Firstly, we introduce the concept of quantum thermalization in ETH formalism and point out two specific cases where ETH is known to break down. Secondly, we discuss the physical meanings of GDOS and have a glance at their properties in the thermodynamic limits following Hartmann et al. (2004); Keating et al. (2015).

In Chapter 3, the TN techniques employed in this thesis are discussed, in particular MPS and MPO in one-dimensional systems. We explain why they are of physical interests through area laws of entanglement and introduce some important algorithms including the variational search of the ground state and time evolution.

In Chapter 4, the main results of this thesis are presented. The kernel polynomial method is first introduced, followed by its combination with TN to calculate the GDOS. We then apply this spectral analysis technique towards thermalization probes and offer three examples: the integrable and non-integrable Ising models and the PXP model.

Finally, we conclude our results in Chapter 5 and propose possible follow-up works.

# Chapter 2

# Backgrounds

## 2.1 Quantum thermalization

The thermalization mechanism of closed quantum systems has been a long time open question. Knowledge from classical statistical physics encourages analogously proposing the *eigenstate thermalization hypothesis* (ETH) (Deutsch, 1991, 2018; Rigol et al., 2008; Srednicki, 1994, 1999), supported by a large amount of theoretical and numerical evidence. It is however already known to fail in some specific cases such like many body localized (MBL) (Abanin et al., 2018; Pal and Huse, 2010) and kinetically constrained (Feldmeier et al., 2019; Lan et al., 2018; Pancotti et al., 2020; Turner et al., 2018a) systems.

### 2.1.1 Eigenstate thermalization hypothesis (ETH)

**Classical thermalization.** We begin with a review on the concept of thermalization in classical statistical physics. Consider a system with $2N$ degrees of freedom in the phase space $\Gamma$. Its evolving trajectory is a curve $\gamma(t) \subset \Gamma$ that depends fully on the initial state $\gamma(0)$ and energy function $E : \Gamma \to \mathbb{R}$. For some observable $O(\gamma(t))$, we want to evaluate its long time average:

$$\bar{O}_t = \lim_{T\to\infty} \frac{1}{T} \int_0^T O(\gamma(t))\mathrm{d}t. \tag{2.1}$$

It is in general a hard problem in the macroscopic case, when $N \gtrsim 10^{23}$. Things can however be simplified assuming *ergodicity*, *i.e.*, given enough long time, $\gamma(t)$ can be arbitrarily close to any point on the equal energy

surface $S \subset \Gamma$. Combining this with Liouville's theorem that the phase space distribution function is a constant along the trajectory, $\bar{O}_t$ can be obtained by averaging over $S$:

$$\bar{O}_t = \frac{\int_S O(p)\mathrm{d}p}{\int_S \mathrm{d}p} =: \bar{O}_{\mathrm{micro},E(\gamma)}, \tag{2.2}$$

which is equal to the classical microcanonical ensemble average.

Those systems without ergodicity are called (Liouville) *integrable*, $N$-dimensional harmonic oscillators being an example. Such a system admits $N$ independent conserved quantities in involution. Its trajectory will be therefore restricted, which is a combination of the $N$ modes and in general quasi-periodic. Any finite dimensional classical system is locally integrable, so integrability is the global behavior of the Hamiltonian. To break integrability is easy, for instance, by adding an anharmonic term. It is believed that the strength of anharmonicity required for erasing the quasi-periodic trajectories becomes vanishingly small when $N \to \infty$ (Falcioni et al., 1991), so in the thermodynamic limit most realistic systems are ergodic.

**Quantum version?** It is natural to ask for a quantum analogy. Can we again claim thermalization in a quantum mechanical system through the equivalence of the long time average and the microcanonical ensemble expectation? Under which conditions is it true?

We should first clarify the definitions. Consider a finite dimensional quantum mechanical system whose Hamiltonian $\hat{H}$ has eigenstate decomposition $\sum_k E_k \left|k\right\rangle \left\langle k\right|$. Choose an initial state $\left|\psi\right\rangle$ that evolves as $\left|\psi(t)\right\rangle = e^{i\hat{H}t}\left|\psi\right\rangle$. The long time average of an observable $\hat{O}$ evaluated for the state $\left|\psi(t)\right\rangle$ is

$$\begin{aligned}
\bar{O}_{t,\psi} &= \lim_{T\to\infty} \frac{1}{T}\int_0^T \left\langle\psi(t)|\hat{O}|\psi(t)\right\rangle \mathrm{d}t \\
&= \lim_{T\to\infty} \frac{1}{T}\sum_{k,k'}\int_0^T \left\langle\psi|k\right\rangle \left\langle k|\hat{O}|k'\right\rangle \left\langle k'|\psi\right\rangle e^{i(E_k-E_{k'})t}\mathrm{d}t \\
&= \sum_{k,k'} \left\langle\psi|k\right\rangle \left\langle k|\hat{O}|k'\right\rangle \left\langle k'|\psi\right\rangle \delta_{E_k,E_{k'}}.
\end{aligned} \tag{2.3}$$

In the non-degenerate case, it can be further simplified to be the *diagonal ensemble* average:

$$\bar{O}_{t,\psi} = \sum_k |\left\langle\psi|k\right\rangle|^2 \left\langle k|\hat{O}|k\right\rangle. \tag{2.4}$$

For the microcanonical ensemble expectation, we need to average over an energy window of width $\Delta E$ around $E_\psi = \langle\psi|\hat{H}|\psi\rangle$, since the spectrum is discrete in the Hilbert space:

$$\bar{O}_{\text{micro},E_\psi} = \frac{1}{n} \sum_{|k\rangle:|E_k - E_\psi|<\Delta E/2} \langle k|\hat{O}|k\rangle \,, \tag{2.5}$$

where $n$ is the number of states in this energy window. The choice of $\Delta E$ depends on the average level spacings $\delta E$ whose inverse, the density of states $g(E)$, defines the thermodynamic entropy $S(E)$: $e^{S(E)} := g(E)$. When the system size $N$ is large, $S(E)$ is usually extensive, *i.e.*, $S(E, N) \approx N \cdot s(E/N)$ for some smooth function $s(\epsilon)$. As a consequence, the average level spacing at certain energy density $\epsilon = E/N$ decreases as $\delta E \propto \exp(-Ns(\epsilon))$. Even for a fixed $\Delta E$, the number of states included in the energy shell grows exponentially with the system size. In the thermodynamic limit, the statistical fluctuations will become negligible.

For Eq. (2.4) and Eq. (2.5) to be equivalent, it is indicated that $O_{kk} = \langle k|\hat{O}|k\rangle$ should fluctuate very little for small variance in energy, i.e., $O_{kk} \approx O_{\text{micro}}(E_k)$, where $O_{\text{micro}}(E)$ is a smooth function. The fluctuations in diagonal elements and the off-diagonal elements should be small compared with the $O_{\text{micro}}(E)$; from a random matrix model it can be further conjectured that both of them are of order $\exp(-S(E)/2)$ (Deutsch, 1991).

**Conjecture 2.1.** *(Energy eigenstate thermalization hypothesis (Srednicki, 1999).) Let $\hat{H} = \sum_k E_k \,|k\rangle\langle k|$ be the Hamiltonian of a non-integrable isolated quantum mechanical system. For a class of observable $\hat{O}$, its elements in the energy eigenstate basis takes the form*

$$O_{k,k'} = O(E_k)\delta_{k,k'} + e^{-S(E)/2} f(\bar{E}, \omega) R_{k,k'}. \tag{2.6}$$

*Here $\bar{E} = (E_k + E_{k'})/2$ and $\omega = E_k - E_{k'}$. $O(E)$ and $f(\bar{E}, \omega)$ are smooth functions of their arguments. The real and imaginary parts of $R_{k,k'}$ are both independent random variables, with zero mean and unit variance.*

*If Eq. (2.6) holds for all energy eigenstates, it is called strong ETH. If an exponentially small fraction of exceptions are allowed, it is called weak ETH.*

There are yet some points ambiguous in the statement. The first is to what class of observables ETH applies. If $\hat{O}$ and $\hat{H}$ commute, $\hat{O}$ does not evolve at all in the Heisenberg picture, let alone thermalize. It is also quite

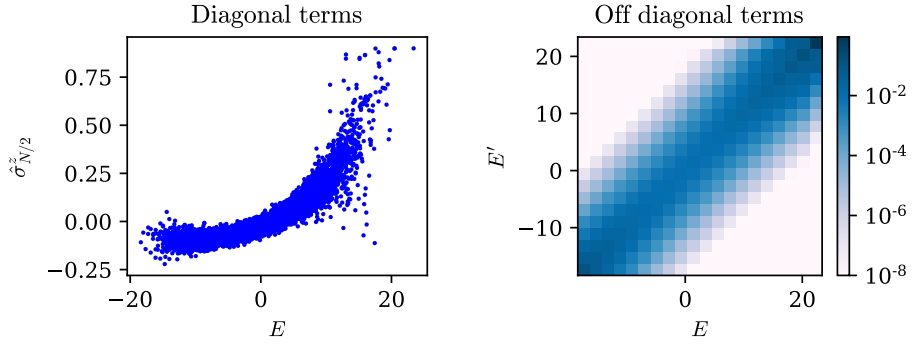


Figure 2.1: Diagonal and off diagonal elements of non-integrable Ising model $\hat{H}_{\text{Ising}} = J\sum_{i=1}^{N-1}\hat{\sigma}_i^z\hat{\sigma}_{i+1}^z + g\sum_{i=1}^{N}\hat{\sigma}_i^x + h\sum_{i=1}^{N}\hat{\sigma}_i^z$ (Eq. (4.39)), where $(J, g, h) = (1, -1.05, 0.5)$. The observable is $\hat{O} = \hat{\sigma}_{N/2}^z$, spin polarization in the middle of the chain. Left: scatter plot of $(E_k, \langle k|\hat{O}|k\rangle)$ for all energy eigenstates. Right: average norm of $\langle k|\hat{O}|k'\rangle$ of corresponding energy blocks in logarithmic scale. System size $L = 14$.

easy to construct other counterexamples given that $\hat{O}$ is highly non-local. ETH is however believed to work for physical local observables (Deutsch, 2018), for instance, those acting on only a few sites in a lattice model.

Another aspect is the definition for *integrability* in quantum systems. The direct quantum analogy of modes in classical Liouville integrability are the energy eigenstates; in this sense all finite dimensional quantum systems are integrable. As ergodicity should be somehow produced, a quantum version of definition is required. Many notions have been proposed, from the aspects of solvability, level spacing statistics, classical limit and so on, but none of the frequently used ones is satisfactory (Gogolin, 2014). The non-integrability in the hypothesis implies the physical behavior, but there is no concise, general and deterministic classification.

Finally, ETH is only a hypothesis. It is known to fail for MBL and kinetically constrained systems, which will be discussed in the next section. Moreover, whether ETH is necessary for thermalization is also unclear, though so far no counterexample has been found in extensive numerical tests of small quantum lattice systems (D'Alessio et al., 2016).

### 2.1.2 Breakdown of ETH

Regardless of the debate in definition of integrability, non-interacting systems and exactly solvable models are generally believed to be quantum integrable. Their avoidance of thermalization is however unstable and sensitive to small (interacting) perturbations (D'Alessio et al., 2016). Another known mechanism to break thermalization is MBL, which is in contrast robust.

MBL follows the idea of Anderson localization (Anderson, 1958) for a single particle that strong disorder provided by external potential leads to insulating behavior. It turns to MBL when turning on interactions. The most famous example is the Heisenberg model with random disorder (Pal and Huse, 2010):

$$\hat{H} = J \sum_{i=1}^{N-1} \hat{\boldsymbol{S}}_i \cdot \hat{\boldsymbol{S}}_{i+1} + \sum_{i=1}^{N} h_i \hat{S}_i^z, \tag{2.7}$$

where $h_i$ are independent random parameters whose distribution is uniform in $[-h, h]$. A phase transition point is observed at $h/J \approx 3.5$ for infinite temperature (Luitz et al., 2015). With strong disorder, large fluctuations of $(S_i^z)_{k,k}$ for adjacent energy eigenstates mark the failure of ETH. Other evidences of entering the localized phase from thermalization include level statistics from Wigner-Dyson form to Poisson distribution (Pal and Huse, 2010), entanglement entropy of highly-excited energy eigenstates from volume law to area law (Serbyn et al., 2013), logarithmic spreading of entanglement instead of power-law spreading from a non-entangled initial state (Bardarson et al., 2012) and so on.

Robustness is an important feature of MBL that distinguishes it from integrable systems. Disorder protects from decoherence some information of the initial states, for instance encoded imbalance or topological order (Huse et al., 2013), which indicates the application of MBL in quantum information storage and processing. Experiments have been done with ultracold atoms in one- (Schreiber et al., 2015) and two- (Choi et al., 2016) dimensional lattices, where long time preserved imbalance between the atoms on even and odd sites of a one-dimensional chain is observed.

Many questions still remain open for MBL. How does the system behave in the transition region? Is disorder required in MBL? Concerning the last one, violation of ergodicity can be realized in translationally invariant systems by constraining the Hilbert space, for example in the PXP

model (Turner et al., 2018a), quantum dimers (Feldmeier et al., 2019; Lan et al., 2018) and the quantum east model (Pancotti et al., 2020; van Horssen et al., 2015). The PXP model is an effective model for Rydberg atom chains that are constrained by strong repulsion of nearest neighbor excited atoms. Many body revivals of an initial Néel state after a quench has been found in experiments (Bernien et al., 2017), which prompted the exploration of non-thermal, so-called scar states (Turner et al., 2018a). PXP model only breaks strong ETH, since the number of scar states (polynomial in system size) is exponentially small among all energy eigenstates.

Numerical studies of ETH and its breakdown are difficult for large systems. Most approaches depend on each energy eigenstate and therefore full diagonalization of the Hamiltonian is required. New theoretical and numerical methods are in need for further explorations.

## 2.2 Generalized density of states (GDOS)

In this thesis, we aim to study the properties of energy eigenstates in a statistical manner by developing algorithms for spectral analysis. It is convenient to first introduce the generalized density of states (GDOS) (Yang et al., 2020) for a finite dimensional Hamiltonian $\hat{H} = \sum_k E_k \left|k\right\rangle \left\langle k\right|$ as

$$g(E, \hat{O}) := \sum_k \delta(E - E_k) \left\langle k|\hat{O}|k\right\rangle = \mathrm{tr}\left[\hat{O}\delta(E - \hat{H})\right]. \tag{2.8}$$

Here $\delta(x)$ is the Dirac delta function. It is a filter that brings only a small energy interval around $E$ into attention. $\hat{O}$ is any operator and different choices lead to a number of physical quantities encoding dynamics of the Hamiltonian:

- $g(E, \mathbb{1})$ is the full density of states (DOS) that counts the density of Hamiltonian eigenstates in energy. It is equivalent to the canonical ensemble partition function up to a Laplace transform: $Z(\beta) = \int e^{-\beta E} g(E, \mathbb{1}) \mathrm{d}E$.

- $g(E, \psi) := g(E, \left|\psi\right\rangle \left\langle\psi\right|) = \sum_k \left|\left\langle\psi|k\right\rangle\right|^2 \delta(E - E_k)$ is the localized density of states (LDOS). It describes the spectral distribution of a state $\left|\psi\right\rangle$ and provides the expectation value $\left\langle\psi|f(\hat{H})|\psi\right\rangle$ for any function $f$

dependent only on the Hamiltonian. Its Fourier transform is connected to the Loschmidt echo, or the survival probability $F(t)$ of the state:

$$F(t) := \left|\langle\psi|e^{-i\hat{H}t}|\psi\rangle\right|^2 = \left|\int g(E,\psi)e^{-iEt}\mathrm{d}E\right|^2. \tag{2.9}$$

Recent research shows that the Loschmidt echo presents different regimes after a quench, which is sensitive towards thermalization (Schiulaz et al., 2019; Távora et al., 2016; Torres-Herrera and Santos, 2015).

- When $\hat{O}$ is an observable, $g(E,\hat{O})$ is the density of states weighted by the expectation values of $\hat{O}$ measured from energy eigenstates. A GDOS can be approximated by a smooth function through broadening the deltas as Gaussians with a narrow width $\sigma$. Denote such smooth functions by $g_\sigma(E,\hat{O})$, which allows the division $O_\sigma(E) := g_\sigma(E,\hat{O})/g_\sigma(E,\mathbb{1})$ as an approximation for the microcanonical ensemble expectation of $\hat{O}$ within an energy shell $[E-\sigma, E+\sigma]$.

  Note that there is some subtle difference difference from the exact microcanonical values, as the weights of states in the energy shell are not equal in this Gaussian type filter. Also states outside the energy interval are given exponentially small weights; this could have a non-negligible effect if taking the DOS into consideration.

### 2.2.1 Thermodynamic limits of GDOS

To have a more concrete idea of GDOS, let us go the thermodynamic limit where some analytical work has been done. In non-interacting systems, the form of DOS is easy to guess according to the central limit theorem, which is a Gaussian. The result can be remarkably extended to all one dimensional short-range interacting spin systems with bounded Hamiltonian, for both LDOS of product states (Hartmann et al., 2004) and the full DOS (Hartmann et al., 2005; Keating et al., 2015). It can be further generalized to any GDOS with a local observable $\hat{O}$.

**LDOS of product states.** In general the LDOS of a state can be of arbitrary shape. For product states in a short range interacting chain, however, they are proved to weakly converge to Gaussians in the thermodynamic

limit. Consider a quantum chain of $N$ sites whose Hamiltonian is bounded and nearest neighbor interacting, *i.e.*,

$$\hat{H}_N = \sum_{i=1}^{N} \hat{\mathcal{H}}_i \tag{2.10}$$

where

$$\hat{\mathcal{H}}_i = \mathbb{1}^{\otimes i-1} \otimes \hat{h}_i \otimes \mathbb{1}^{\otimes N-i} + \mathbb{1}^{\otimes i-1} \otimes \hat{g}_{i,i+1} \otimes \mathbb{1}^{\otimes N-i-1} \tag{2.11}$$

and $||\mathcal{H}_i|| \leq C$ for all $1 \leq i \leq N$. We assume open boundary condition, which means $\hat{g}_{N,N+1} = 0$. Again the spectral decomposition is written as $\hat{H}_N = \sum_k E_k \left|k\right\rangle \left\langle k\right|$. The theorem then holds:

**Theorem 2.2.** *(Gaussian LDOS (Hartmann et al., 2004).) Let* $|a\rangle = \otimes_{i=1}^{N} |a_i\rangle$ *be a product state with mean energy* $E_a = \langle a|\hat{H}|a\rangle$ *and variance* $\sigma_a^2 = \langle a|\hat{H}^2|a\rangle - E_a^2$. *If* $\sigma_a^2 \geq \Delta \cdot N$ *for some constant* $\Delta > 0$, *then the measure defined by LDOS*

$$P_a\left(E \in [E_1, E_2]\right) = \int_{E_1}^{E_2} g(E, a) \mathrm{d}E = \sum_{|k\rangle : E_1 \leq E_k \leq E_2} |\left\langle a|k\right\rangle|^2 \tag{2.12}$$

*converges weakly to normal distribution in the thermodynamic limit:*

$$\lim_{N\to\infty} P_a\left(E \in [E_1, E_2]\right) = \frac{1}{\sqrt{2\pi}\sigma_a} \int_{E_1}^{E_2} \exp\left[-\frac{(E - E_a)^2}{2\sigma_a^2}\right] \mathrm{d}E \tag{2.13}$$

*for any* $-\infty < E_1 < E_2 < \infty$.

The condition $\sigma_a^2 \geq \Delta N$ indicates that the product state is not too close to an energy eigenstate. Since the Hamiltonian is short-range interacting, the variance is indeed upper bounded by $\mathcal{O}(N)$:

$$\begin{aligned} \sigma_a^2 &= \langle a|\hat{H}^2|a\rangle - \langle a|\hat{H}|a\rangle^2 \\ &= \sum_{i,j=1}^{N} \Big( \langle a|\hat{\mathcal{H}}_i \hat{\mathcal{H}}_j|a\rangle - \langle a|\hat{\mathcal{H}}_i|a\rangle \langle a|\hat{\mathcal{H}}_j|a\rangle \Big) \\ &\leq 3C^2 N. \end{aligned} \tag{2.14}$$

Thus the width of the Gaussian is of order $\sqrt{N}$. Since the range of the whole spectrum is extensive with regard to the system size $N$, in the thermodynamic limit the LDOS becomes narrow in energy density.

The main idea of the proof is to split the spin chain into blocks that do not interact with each other and links between them. By showing the contribution of the links vanish as the system size approaches infinity, the Lyapunov's version of central limit theorem can be applied. See Appendix 6.1.1 for details.


Figure 2.2: Chain splitting.

**DOS.** The structure of the proof does not change much in the DOS version of theorem (Hartmann et al., 2005; Keating et al., 2015) for a spin-1/2 chain, which states

$$\lim_{N\to\infty}\int_{E_1}^{E_2} g(E,\mathbb{1})\mathrm{d}E = \frac{2^N}{\sqrt{2\pi N}\alpha}\int_{E_1}^{E_2} e^{-E^2/2N\alpha^2}\mathrm{d}E. \tag{2.15}$$

$\alpha$ is defined in the additional normalization condition

$$\frac{1}{2^N}\mathrm{tr}\left(\hat{H}_N^2\right) = N\alpha^2. \tag{2.16}$$

It suggests nothing new but bounded operators. The othonormal Pauli basis $\hat{\sigma}^{(a)}$ $(a=0,1,2,3)$ can be chosen for hermitian operators in the local Hilbert space, and the most general traceless local Hamiltonian in Eq. (2.11) can be written explicitly as

$$\hat{\mathcal{H}}_i = \sum_{a=0}^{3}\sum_{b=1}^{3}\alpha_{a,b,i}\hat{\sigma}_i^{(a)}\hat{\sigma}_{i+1}^{(b)} \tag{2.17}$$

when $1 < i < N$ and $\alpha_{i,a,b}$ are real parameters. That the Hamiltonian is locally bounded leads to $|\alpha_{a,b,i}| < C'$ for some constant $C'$. The trace of Hamiltonian squared can therefore be computed:

$$\frac{1}{2^N}\mathrm{tr}\left(\hat{H}_N^2\right) = \sum_{i=1}^{N}\sum_{a=0}^{3}\sum_{b=1}^{3}\alpha_{a,b,i}^2 =: N\alpha^2. \tag{2.18}$$

Similar to the LDOS case, in the thermodynamic the DOS weakly converges to a Gaussian that is narrow in energy density. Most of the states are squeezed around $\epsilon = E/N = 0$, which corresponds to the infinite temperature from canonical ensemble view.

**GDOS of local observables.** We further general the theorem for GDOS of local observables. Let $\hat{O}$ be a local spin-1/2 hermitian operator for $s$ neighboring sites with eigenspace decomposition

$$\hat{O} = \sum_{m=1}^{2^s} \tilde{O}_m \hat{P}_m. \tag{2.19}$$

$\tilde{O}_m \in \mathbb{R}$ are its eigenvalues and $\hat{P}_m$ are projectors onto corresponding eigenspaces. We want to measure $\hat{O}$ on a spin-1/2 chain of length $N$ from the $q_N$-th site, with $\hat{O}_N = \mathbb{1}^{\otimes q_N} \otimes \hat{O} \otimes \mathbb{1}^{\otimes N-q_N-s}$ and $\hat{P}_{N,m} = \mathbb{1}^{\otimes q_N} \otimes \hat{P}_m \otimes \mathbb{1}^{\otimes N-q_N-s}$.

**Theorem 2.3.** *(GDOS as a sum of Gaussians.) If the limit*

$$\lim_{N\to\infty} \mathrm{tr}\left( \sum_{j=q_N-1}^{q_N+s} \mathcal{H}_j \hat{P}_{N,m} \right) = E_m \tag{2.20}$$

*exists for all $m$, then*

$$\lim_{N\to\infty} \int_{E_1}^{E_2} g(E, \hat{O}_N) \mathrm{d}E = \frac{2^{N-s}}{\sqrt{2\pi N}\alpha} \sum_m \tilde{O}_m \int_{E_1}^{E_2} e^{-(E-E_m)^2/2N\alpha^2} \mathrm{d}E \tag{2.21}$$

*for any $-\infty < E_1 < E_2 < \infty$.*

The details of the proof are shown in Appendix 6.1.2. Note that DOS is a special case when $\hat{O} = \mathbb{1}$.

### 2.2.2 Remarks

**Equivalence of microcanonical and canonical ensemble.** This form of DOS allows us to argue the equivalence of microcanonical and canonical ensembles assuming ETH. The canonical ensemble density operator, or Gibbs

state expectation of a (local) observable $\hat{O}$ at inverse temperature $\beta$ reads in the thermodynamic limit

$$\begin{aligned}\bar{O}_{\mathrm{Gibbs},\beta} &= \frac{\mathrm{tr}\left(\hat{O}e^{-\beta\hat{H}}\right)}{\mathrm{tr}\left(e^{-\beta\hat{H}}\right)} = \frac{\sum_k \langle k|\hat{O}|k\rangle\, e^{-\beta E_k}}{\sum_k e^{-\beta E_k}} = \frac{\sum_k O(E_k)e^{-\beta E_k}}{\sum_k e^{-\beta E_k}} \\ &\approx \frac{\int O(E)e^{-\beta E}g(E,\hat{\mathbb{1}})\mathrm{d}E}{\int e^{-\beta E}g(E,\hat{\mathbb{1}})\mathrm{d}E} \\ &\approx \frac{1}{\sqrt{2\pi N}\alpha}\int O(E)\exp\left[-\frac{1}{2N\alpha^2}\left(E+N\alpha^2\beta\right)^2\right]\mathrm{d}E \\ &\approx O(-N\alpha^2\beta).\end{aligned} \tag{2.22}$$

It is $O(E)$ (defined in Eq. (2.6)) averaged over an effective Gaussian distribution peaked at $E_\beta = -N\alpha^2\beta \propto N\beta$, whose width $\alpha\sqrt{N}$ is narrow in energy density. In the thermodynamic limit, $\bar{O}_{\mathrm{Gibbs},\beta}$ is exactly the microcanonical values at energy density $\epsilon = -\alpha^2\beta$, given that it does not exceed the range of the spectrum.

**Effects on Gaussian-type filters.** In section 2.2, we introduce the approximation of $\delta$-filters as Gaussians

$$\delta_\sigma(E-\hat{H}) \approx \frac{1}{\sqrt{2\pi}\sigma}\exp\left[-(E-\hat{H})^2/2\sigma^2\right]. \tag{2.23}$$

The unbalanced distribution of states will however lead to an effective shift for the center of the filter, following a similar analysis. Again, assuming ETH and in the thermodynamic limit

$$\begin{aligned}O_\sigma(E) &= \frac{\mathrm{tr}\left(\hat{O}e^{-(E-\hat{H})^2/2\sigma^2}\right)}{\mathrm{tr}\left(e^{-(E-\hat{H})^2/2\sigma^2}\right)} = \frac{\int O(\tilde{E})e^{-(E-\tilde{E})^2/2\sigma^2}g(\tilde{E},\mathbb{1})\mathrm{d}\tilde{E}}{\int e^{-(E-\tilde{E})^2/2\sigma^2}g(\tilde{E},\mathbb{1})\mathrm{d}\tilde{E}} \\ &\approx \frac{\sqrt{\sigma^2+N\alpha^2}}{\sqrt{2\pi N}\sigma\alpha}\int O(\tilde{E})e^{-\left(\frac{1}{2N\alpha^2}+\frac{1}{2\sigma^2}\right)\left(\tilde{E}-\frac{E}{1+\sigma^2/N\alpha^2}\right)}\mathrm{d}\tilde{E} \\ &\approx O\left(\frac{E}{1+\sigma^2/N\alpha^2}\right).\end{aligned} \tag{2.24}$$

As a consequence, $\sigma = o(\sqrt{N})$ has to be satisfied in order to obtain the desired microcanonical values.

**Application to Ising chain.** Let us now consider a concrete example, the quantum Ising model. Its Hamiltonian is

$$\hat{H}_{\text{Ising}} = J\sum_{i=1}^{N-1}\hat{\sigma}_i^z\hat{\sigma}_{i+1}^z + g\sum_{i=1}^{N}\hat{\sigma}_i^x + h\sum_{i=1}^{N}\hat{\sigma}_i^z, \tag{2.25}$$

for which $\alpha = \sqrt{J^2+g^2+h^2}$. The quantum Ising model is known to be non-integrable when $g$ and $h$ are both nonzero, and we choose $(J,g,h) = (1,-1.05,0.5)$ for illustration.

In the upper and middle plots of Fig. 2.3, the DOS $g(E,\mathbb{1})$ and GDOS $g(E,\hat{\sigma}_N^z)$ are presented respectively. The eigenspace decomposition of $\hat{O}_N = \hat{\sigma}_{N/2}^z$ gives $\hat{P}_\pm = (\mathbb{1}\pm\hat{\sigma}^z)/2$ and $\tilde{O}_\pm = \pm 1$. One can compute $E_\pm = \text{tr}\left(\hat{H}_{\text{Ising}}\hat{P}_{N,\pm}\right) = \pm h$, and hence

$$g(E,\hat{\sigma}_{N/2}^z) \sim \frac{2^{N-1}}{\sqrt{2\pi N}\alpha}\left[e^{-\frac{(E-h)^2}{2N\alpha^2}} - e^{-\frac{(E+h)^2}{2N\alpha^2}}\right]. \tag{2.26}$$

Eq. (2.26) in good agreement with with the numerical results by Chebyshev expansion that will be introduced in Chapter 4.

With the success in computing GDOS, one may ask: is it possible to also compute the microcanonical ensemble expectation in the thermodynamic limit in this analytical way? Unfortunately, the answer is *no*. From Eq. (2.15) and Eq. (2.26), the division $g(E,\hat{O})/g(E,\mathbb{1})$ reads

$$\begin{aligned}\frac{g(E,\hat{\sigma}_{N/2}^z)}{g(E,\mathbb{1})} &\overset{?}{\approx} \frac{2^{N-1}}{\sqrt{2\pi N}\alpha}\left[e^{-\frac{(E-h)^2}{2N\alpha^2}} - e^{-\frac{(E+h)^2}{2N\alpha^2}}\right] \Big/ \frac{2^N}{\sqrt{2\pi N}\alpha}\exp\left(-\frac{E^2}{2N\alpha^2}\right) \\ &= \exp\left(-\frac{h^2}{2N\alpha^2}\right)\sinh\left(\frac{hE}{N\alpha^2}\right) \approx \sinh\left(\frac{h}{\alpha^2}\epsilon\right).\end{aligned} \tag{2.27}$$

In the ETH regime the microcanonical and canonical ensembles should be equivalent in the thermodynamic limit, which will be numerically verified in section 4.3.1. Eq. (2.27) and canonical values calculated by matrix product density operators (details in 3.4.2) are shown in in the lower panel of Fig. 2.3 for comparison. The system size $N = 80$, where the shapes of both curves as a function of energy density $\epsilon$ have converged. The expected agreement of the two curves, however, does not occur. They are only tangent at zero energy density, namely infinite temperature, where the DOS peaks.

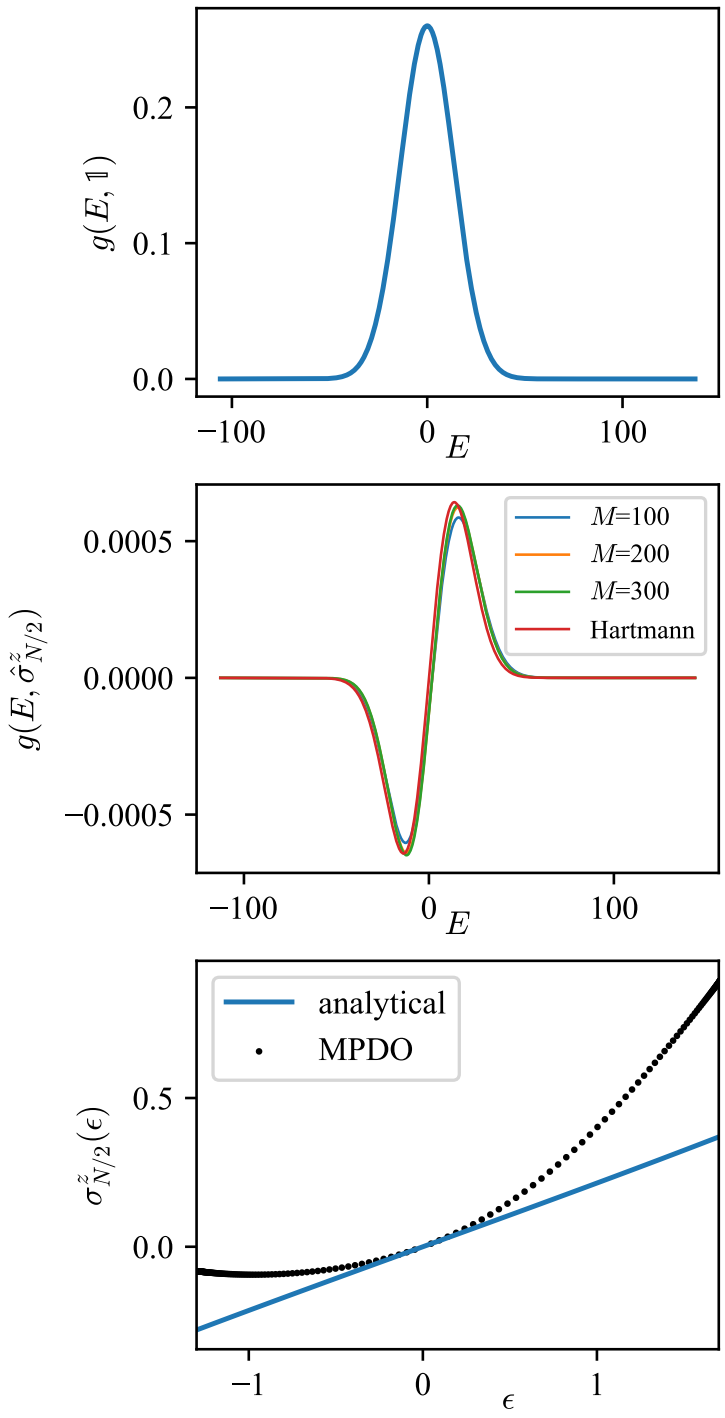


Figure 2.3: **Upper**: Rescaled DOS $g(E, \mathbb{1})/2^N$ from Hartmann's approach. **Middle**: Rescaled GDOS $g(E, \hat{\sigma}^z_{N/2})/2^N$. The red curve is from Eq. (2.26), while the others are numerical results by Chebyshev expansion up to the $M$-th order. **Lower**: The blue curve is from Eq. (2.27), while the black scatters are Gibbs ensemble expectation of $\hat{\sigma}^z_{N/2}$. For all plots, $N = 80$.

The theorems above only provide a weak convergence of probability measure. Since the width of DOS distribution, scaling as $1/\sqrt{N}$ in energy density $\epsilon$, shrinks to a point in the thermodynamic limit, it *fails* to predict $O(E)$ at any finite $\epsilon$. There are however rich physics at finite temperatures, which requires further numerical analysis.

# Chapter 3

# Tensor Network Techniques

## 3.1 Area laws and tensor networks

Very few quantum mechanical systems are exactly solvable. In a quantum many body system, the dimension of its Hilbert space grows exponentially with the system size. Therefore to numerically solve such systems, we have to diagonalize a (sparse) hermitian matrix with exponentially large dimension.

Entanglement between different degrees of freedom adds to the complexity. In the contrary, localized states without entanglement, serving as eigenstates of non-interacting Hamiltonians, can be expressed as tensor products. As a matter of fact, many states of physical interest, including ground states and thermal states, do not involve much entanglement but instead obey the area law (Eisert et al., 2010): the entanglement of a bipartition $\{ A, B \}$ of a large system $A \sqcup B$ scales as the size of boundary between $A$ and $B$. This is a small region of the whole Hilbert space, and there could be more efficient ways to parameterize such states.

The way to quantify this correlation for a bipartite state is to use the von Neumann entanglement entropy (Bennett et al., 1996)

$$S(\rho_A) := -\mathrm{tr}\,(\rho_A \ln \rho_A) = S(\rho_B), \tag{3.1}$$

where the reduced density matrix $\rho_A := \mathrm{tr}_B(\rho_{AB})$ is given by the partial trace of a density operator $\rho_{AB}$ of the whole system $A \sqcup B$. For a pure state $|\psi\rangle$, $\rho_{AB} = |\psi\rangle\langle\psi|$. The entanglement entropy of a state that obeys the area law is proportional to the area of the boundary $\partial A$:

$$S(\rho_A) \propto |\partial A|\,. \tag{3.2}$$

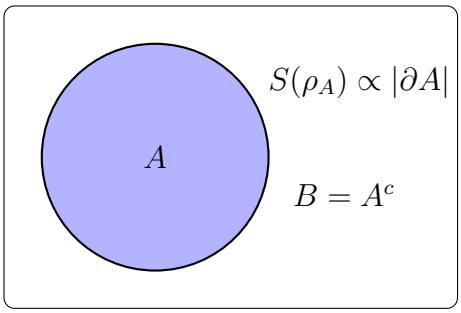


Figure 3.1: Area law.

The ground states of gapped, locally interacting Hamiltonians are shown to be of this class in one-dimensional systems, where $S(\rho_A)$ is bounded by $\mathcal{O}\left((\ln d)^3/\Delta\right)$ (Hastings, 2007; Verstraete and Cirac, 2006). $d$ is the local Hilbert space dimension and $\Delta$ is the gap between the ground state and the first excited state. A non-vanishing gap $\Delta$ in the thermodynamic limit indicates a finite correlation length; otherwise the system would be critical. In higher dimensions, it is currently a widely-believed conjecture without a general proof. Another version of area law for mutual information of Gibbs states $\rho \propto \exp(-\beta \hat{H})$,

$$I(A:B) = S(\rho_A) + S(\rho_B) - S(\rho) \leq c\beta|\partial A| \tag{3.3}$$

where $c$ is some constant, has however been proved for any spatial dimensions (Wolf et al., 2008).

*Projected entangled pair state* (PEPS) (Verstraete and Cirac, 2004) are natural representations for the states of spin systems that satisfy area laws. They are defined on lattices of any spatial dimension, whose edge $e = \{i, j\} \in E$ each support a $D_e$-dimensional maximally entangled spin pair between nearest neighboring sites $i$ and $j$:

$$|\phi\rangle_e = \sum_{a_e=1}^{D_e} |n\rangle_{i,j} \otimes |n\rangle_{j,i}\,. \tag{3.4}$$

At each lattice site $v \in V$, a tensor linearly and locally projects the $D_e$-dimensional auxiliary spins, entangled with $k$ neighbors of the site and labelled by $a_e$, to a $d$-dimensional physical spin $s_v$:

$$M_v = (M_v)^{s_v}_{a_{e_1}\cdots a_{e_k}} : \bigotimes_{e|e\cap v\neq\varnothing} \mathbb{C}^{D_e} \to \mathbb{C}^d. \tag{3.5}$$

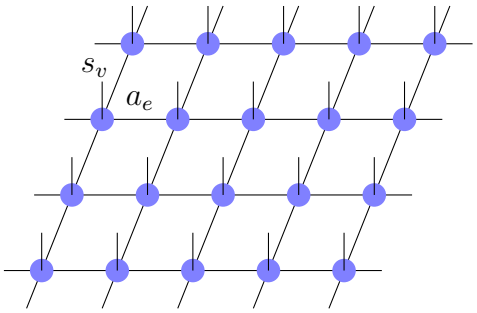


Figure 3.2: Graphical representation of PEPS on a 2D square lattice.

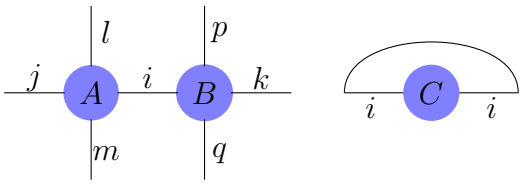


Figure 3.3: Tensor contraction.

Finally, the state is defined as

$$|\psi\rangle = \bigotimes_{v\in V} M_v \left( \bigotimes_{e\in E} |\phi\rangle_e \right). \tag{3.6}$$

$|\psi\rangle$ is named a PEPS according to its construction, graphically represented in Fig. 3.2. At each site of the lattice lives a tensor, and a *leg* represents an index of the local tensor. When two legs of a tensor are connected, the corresponding indices are traced out; the right side of Fig. 3.3 represents $\sum_i C_{ii}$. Two tensors can be contracted in this way, for instance the new tensor in the left side of Fig. 3.3 represents $\sum_i A_{lmji} B_{pqik}$. The remaining untraced legs in a PEPS label the physical dimensions.

$D_e$ are called *bond dimensions* which characterize the maximal entanglement a PEPS can carry. If we modify the tensor such that the auxiliary spins are mapped to a $d$-dimensional operator, the resulting operator is called a *projected entangled pair operator* (PEPO). In this thesis, we always focus on the 1D case, where there are only two auxiliary spins at each site and the tensors are reduced to matrices labelled by physical spins. PEPS and PEPO are therefore specialized to matrix product states (MPS) and matrix product operators (MPO), respectively.

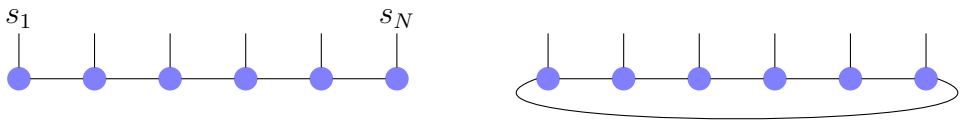


Figure 3.4: Graphical representation of MPS with OBC (left) and PBC (right).

## 3.2 Matrix product states (MPS)

MPS was first introduced in (Accardi, 1981) to describe quantum Markov chains. It serves as the ground state of the AKLT Hamiltonian (Affleck et al., 1987), where spin-1/2 singlets are distributed on the edges and two half integer spins are projected to a spin-1 particle at each site. Later, after the success of density matrix renormalization group (DMRG) algorithm (White, 1992, 1993) in simulating spin chains, it is found to be a variational method working in the MPS manifold (Dukelsky et al., 1998; Östlund and Rommer, 1995; Verstraete et al., 2004b). Now MPS is a standard variational ansatz to calculate ground states of 1D spin systems.

As discussed in the previous section, an MPS in a spin chain of $N$ sites can be formulated as

$$|\psi\rangle = \sum_{\boldsymbol{s}} \mathrm{tr}\left(M_1^{s_1} \cdots M_N^{s_N}\right) |\boldsymbol{s}\rangle \,. \tag{3.7}$$

$\boldsymbol{s} = (s_1, \cdots, s_N) \in \mathbb{Z}_d^N$ are spin indices with physical dimension $d$. $M_n^{s_n}$ are $D_{n-1} \times D_n$ dimensional complex matrices for $1 \leq n \leq N$ with bond dimensions $\boldsymbol{D}$, where $D_0 = D_N$. Under open boundary conditions (OBC), $D_N = 1$, which means $M_1^{s_1}$ is a row vector and $M_N^{s_N}$ is a column vector; while with periodic boundary conditions (PBC), $D_N > 1$.

### 3.2.1 Canonical form

Any state of such spin chains can be brought into MPS form through singular value decompositions (SVD). The SVD allows the decomposition of any complex matrix $M \in \mathbb{C}^{m \times n}$

$$M = U \Lambda V^\dagger \tag{3.8}$$

such that $\Lambda$ is a non-negative $m \times n$ dimensional diagonal matrix and $U$, $V$ are unitary matrices. Without loss of generality, we assume the diagonal

values of $\Lambda$ are sorted as $\lambda_1 \geq \cdots \geq \lambda_k \geq 0$, where $k = \min(m, n)$. SVD is also called the Schmidt decomposition when applied to a bipartition $\{ A, B \}$ of a quantum system:

$$\begin{aligned} |\phi\rangle_{AB} &= \sum_{a,b} M_{ab} |a\rangle \otimes |b\rangle = \sum_{p,a,b} U_{ap} \Lambda_{pp} V^\dagger_{pb} |a\rangle \otimes |b\rangle \\ &= \sum_p \lambda_p \left( \sum_a U_{ap} |a\rangle \right) \otimes \left( \sum_b V^*_{bp} |b\rangle \right). \end{aligned} \tag{3.9}$$

Here $|\phi\rangle_{AB}$ is a general pure state of $A \sqcup B$, while $|a\rangle$ and $|b\rangle$ are orthonormal bases of the subsystems $A$ and $B$ respectively. The diagonal elements of $\Lambda$ are thus square roots of the eigenvalues of the reduced density matrix $\rho_A = \mathrm{tr}_B |\phi\rangle_{AB} \langle\phi|_{AB} = \sum_p \lambda_p^2 |p\rangle_A \langle p|_A$, where $|p\rangle_A = \sum_a U_{ap} |a\rangle$.

Now consider the most general form of states

$$|\varphi\rangle = \sum_{\boldsymbol{s}} \varphi_{\boldsymbol{s}} |\boldsymbol{s}\rangle . \tag{3.10}$$

The first spin can be taken out of the tensor $\varphi_{s_1,\cdots,s_N}$ by doing an SVD

$$\begin{aligned} \varphi_{s_1,\cdots,s_N} = \varphi^{(1)}_{s_1,(s_2\cdots s_N)} &= \sum_{a_1} \underbrace{U^{(1)}_{s_1,a_1}}_{A_1} \underbrace{\Lambda^{(1)}_{a_1,a_1} V^{\dagger(1)}_{a_1,(s_1\cdots s_N)}}_{\varphi^{(2)}} \\ &=: \sum_{a_1} (A_1^{s_1})_{a_1} \varphi^{(2)}_{(a_1 s_2),(s_3\cdots s_N)}. \end{aligned} \tag{3.11}$$

Then the second:

$$\begin{aligned} \varphi^{(2)}_{(a_1 s_2),(s_3\cdots s_N)} &= \sum_{a_2} \underbrace{U^{(1)}_{(a_1 s_2),a_2}}_{A_2} \underbrace{\Lambda^{(2)}_{a_2,a_2} V^{\dagger(2)}_{a_2,(s_3\cdots s_N)}}_{\varphi^{(3)}} \\ &=: \sum_{a_2} (A_2^{s_2})_{a_1,a_2} \varphi^{(3)}_{(a_2 s_3),(s_4\cdots s_N)}. \end{aligned} \tag{3.12}$$

This process can be recursively done from left to right, until

$$\varphi_{s_1,\cdots,s_N} = \sum_{a_1,\cdots,a_{N-1}} (A_1^{s_1})_{a_1} (A_2^{s_2})_{a_1,a_2} \cdots \left(A_{N-1}^{s_{N-1}}\right)_{a_{N-2},a_{N-1}} (A_N^{s_N})_{a_{N-1}} , \tag{3.13}$$

where $(A_N^{s_N})_{a_{N-1}} := \varphi^{(N)}_{a_{N-1},s_N}$.

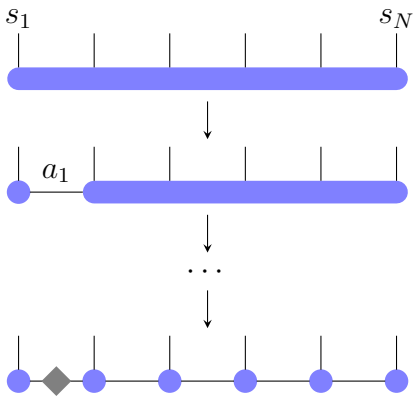


Figure 3.5: Bringing a general state to a left-canonical MPS by SVD.

Note that the properties of the SVD ensure

$$\sum_{s_n=1}^{d} A_n^{s_n\dagger} A_n^{s_n} = \mathbb{1}. \tag{3.14}$$

for any $1 \leq n \leq N$. This is called the *left-canonical form* of MPS. The same procedure can be done starting from the right, which generates a *right-canonical* MPS, for which the matrices satisfy:

$$\sum_{s_n=1}^{d} B_n^{s_n} B_n^{s_n\dagger} = \mathbb{1}. \tag{3.15}$$

We use $B$ to label the matrices with the right-canonical gauge conditions to distinguish from those $A$ matrices with left-canonical gauge conditions. In this case, the diagonal fixed point (singular values of the last SVD, illustrated as a grey diamond in Fig. 3.5) will move from the left end to the right end of the chain.

### 3.2.2 Truncation of MPS

The singular values $\lambda_p^{(n)}$ in the construction of canonical MPS indicates whether there is redundancy in the bond dimension. Those dimensions with zero (or small enough) singular values can be trimmed with no (or tolerable) loss of accuracy. To better understand this cutoff, let us consider an MPS of

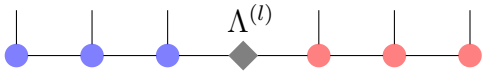


Figure 3.6: Bipartition of MPS in mixed canonical form.

*mixed-canonical* form:

$$|\psi\rangle = \sum_{\boldsymbol{s}} A_1^{s_1} \cdots A_l^{s_l} \Lambda^{(l)} B_{l+1}^{s_{l+1}} \cdots B_N^{s_N} |\boldsymbol{s}\rangle \,. \tag{3.16}$$

For a mixed-canonical MPS, the SVD are applied from both ends of the chain, and the diagonal $\Lambda^{(l)}$ lies between any neighboring sites. It cuts the chain into two parts: matrices in the left are in left-canonical form, while those in the right are in right-canonical form. The Schmidt decomposition of $|\psi\rangle$ for the bipartition $A = \{1, \cdots, l\}$, $B = \{l+1, \cdots, N\}$ then follows from Eq. (3.9). $\left(\lambda_p^{(l)}\right)^2$ serves as the eigenvalues of the reduced density matrix, and the corresponding von Neumann entanglement entropy is therefore bounded by the bond dimension $D_l$:

$$S(\rho_A) = -\sum_p \left(\lambda_p^{(l)}\right)^2 \ln \left(\lambda_p^{(l)}\right)^2 \leq -D_l \cdot \left(\frac{1}{D_l} \ln \frac{1}{D_l}\right) = \ln D_l. \tag{3.17}$$

Let us denote an MPS with maximum bond dimension $D$ by $|\psi^{(D)}\rangle$. Note that there is some subtlety in the approximability of a state by an MPS, which depends on the Rényi entropy

$$S_\alpha(\rho) = \frac{\ln \mathrm{tr}\rho^\alpha}{1-\alpha}, \quad 0 \leq \alpha \leq \infty. \tag{3.18}$$

The Rényi entropy is a generalization of von Neumann entropy: $\lim_{\alpha \to 1} S_\alpha(\rho) = S(\rho)$. It is only proved that a state whose Rényi entropy with $\alpha < 1$ scales as a constant or $\ln N$ can be efficiently approximated by an MPS (Schuch et al., 2008; Verstraete and Cirac, 2006).

The bond dimensions grow quickly when we perform certain operations on MPS. For instance, if we want to add up two MPS $|\psi_1^{(D_1)}\rangle$ and $|\psi_2^{(D_2)}\rangle$, each new matrix should be a direct sum of the original two matrices at the same site

$$(M_n^{s_n})' = \begin{pmatrix} (M_n^{s_n})_1 & 0 \\ 0 & (M_n^{s_n})_2 \end{pmatrix} \tag{3.19}$$

such that

$$\mathrm{tr}\left[(M_1^{s_1}\cdots M_N^{s_N})'\right] = \mathrm{tr}\begin{pmatrix}(M_1^{s_1}\cdots M_N^{s_N})_1 & 0\\ 0 & (M_1^{s_1}\cdots M_N^{s_N})_2\end{pmatrix}. \tag{3.20}$$

The resulting bond dimension is therefore $D_1+D_2$. In numerical calculations, MPS should be kept compressed in order not to exceed the limits of computing resources. To approximate an MPS $|\psi^{(D)}\rangle$ with $|\tilde{\psi}^{(\tilde{D})}\rangle$, where $D > \tilde{D}$, the distance

$$\begin{aligned}&\left|\left||\psi^{(D)}\rangle - |\tilde{\psi}^{(\tilde{D})}\rangle\right|\right|_2^2\\ &= \langle\psi^{(D)}|\psi^{(D)}\rangle - \langle\psi^{(D)}|\tilde{\psi}^{(\tilde{D})}\rangle - \langle\tilde{\psi}^{(\tilde{D})}|\psi^{(D)}\rangle + \langle\tilde{\psi}^{(\tilde{D})}|\tilde{\psi}^{(\tilde{D})}\rangle\end{aligned} \tag{3.21}$$

should be minimized. Take the partial derivative with regard to the complex conjugate of a matrix element $(\tilde{M}_n^{s_n})^*_{a'_{n-1},a'_n}$ of $|\tilde{\psi}^{(\tilde{D})}\rangle$, which can be viewed as a tensor of three indices $s_n$, $a'_{n-1}$ and $a'_n$:

$$\frac{\partial}{\partial\left(\tilde{M}_n^{s_n}\right)^*_{a'_{n-1},a'_n}}\left|\left||\psi^{(D)}\rangle - |\tilde{\psi}^{(\tilde{D})}\rangle\right|\right|_2^2$$

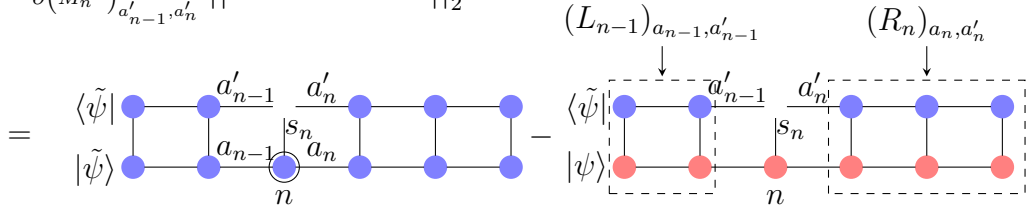


$$= \sum_{a_{n-1},a_n} P_{(a'_{n-1}a'_n),(a_{n-1}a_n)}(\tilde{M}_n^{s_n})_{a_{n-1}a_n} - \qquad b^{s_n}_{a'_{n-1}a'_n} \tag{3.22}$$

That Eq. (3.22) $= 0$ can be reduced to a $\tilde{D}^2 \times \tilde{D}^2$ dimensional linear equation for $\tilde{M}_n^{s_n}$:

$$\sum_{a_{n-1},a_n} P_{(a'_{n-1}a'_n),(a_{n-1}a_n)}(\tilde{M}_n^{s_n})_{a_{n-1}a_n} = b^{s_n}_{a'_{n-1}a'_n}. \tag{3.23}$$

The $P$ tensor in the left hand side is the contraction of $\langle\tilde{\psi}|$ and $|\tilde{\psi}\rangle$ leaving out the matrices at site $n$:

$$\begin{aligned}&P_{(a'_{n-1}a'_n),(a_{n-1}a_n)}\\ &= \sum_{\substack{s_1,\cdots,s_{n-1},s_{n+1},\cdots,s_N\\ a_1,\cdots,a_{n-2},a_{n+1},\cdots,a_{N-1}\\ a'_1,\cdots,a'_{n-2},a'_{n+1},\cdots,a'_{N-1}}} \prod_{1\le l\le N, l\neq n}\left(\tilde{M}_l^{s_l}\right)_{a_{l-1},a_l}\left(\tilde{M}_l^{s_l}\right)^*_{a'_{l-1},a'_l}.\end{aligned} \tag{3.24}$$

Where $a_0 = a_N = 1$ in the open boundary condition. Similarly, the right hand side reads

$$b^{s_n}_{a'_{n-1}a'_n} = \sum_{\substack{s_1,\cdots,s_{n-1},s_{n+1},\cdots,s_N \\ a_1,\cdots,a_{N-1} \\ a'_1,\cdots,a'_{n-2},a'_{n+1},\cdots,a'_{N-1}}} \left[ (M^{s_n}_n)_{a_{n-1},a_n} \cdot \prod_{1\le l\le N, l\neq n} (M^{s_l}_l)_{a_{l-1},a_l} \left(\tilde{M}^{s_l}_l\right)^*_{a'_{l-1},a'_l} \right]. \tag{3.25}$$

If $|\tilde{\psi}^{(D)}\rangle$ is kept in mixed-canonical form centered at $n$, the $P$ tensor is actually an identity map and hence there is no need to solve the linear system:

$$(M^{s_n}_n)_{a'_{n-1}a'_n} = b^{s_n}_{a'_{n-1}a'_n}. \tag{3.26}$$

With Eq. (3.26), one can follow the steps below to variationally truncate the MPS $|\psi^{(D)}\rangle$:

1. Start with a trial function $|\tilde{\psi}^{(\tilde{D})}_0\rangle$ in left-canonical form.
2. Sweep from the right end of the chain to the left, each time update the matrix at the current site with Eq. (3.26) and do SVD to ensure the mixed-canonical form for the next step. The MPS becomes right-canonical when reaching the left end.
3. Sweep from the left to the right, which brings the resulting MPS to left-canonical form again.
4. Repeats 2 and 3 until the error $\left|\left||\psi^{(D)}\rangle - |\tilde{\psi}^{(\tilde{D})}\rangle\right|\right|^2_2$ has converged or pre-specified rounds of sweeps have been done.

The tensor $b^{s_n}_{a'_{n-1},a'_n}$ has two components: $R_n$ as defined in Eq. (3.22) and similarly $L_{n-1}$ that starts from the left. In each sweep, the tensors $L_n$ ($R_n$) can be calculated iteratively from $R_{n+1}$ ($L_{n-1}$, respectively). In the sweep from right the left, for example, all the $L_n$ can be stored so that they only need to be calculated once; hence the time cost of contraction is $\mathcal{O}(NdD^3)$ for each sweep. As the SVD of a $D \times dD$-dimensional matrix is also $\mathcal{O}(D^3 d)$, the total time complexity of this algorithm is $\mathcal{O}(NdD^3)$ per sweep.

This algorithm can be generalized to approx the sum of several MPS with a single one, which only requires adding all the $b$ tensors of the corresponding initial MPS in Eq. (3.26).

## 3.3 Matrix product operators (MPO)

It is natural to write an MPO analogously to an MPS as

$$\hat{O}^{(D)} = \sum_{\boldsymbol{s},\boldsymbol{s}'} \mathrm{tr}\left(M_1^{s_1,s_1'} \cdots M_1^{s_N,s_N'}\right) |\boldsymbol{s}\rangle \langle \boldsymbol{s}'| \,. \tag{3.27}$$

There are now two physical indices for each matrix instead one. When an MPO is applied to an MPS (MPO, respectively), the resulting state (operator) is still an MPS (MPO) whose bond dimension will be the product of the original ones. Luckily, the compression algorithm is still applicable for MPO, since an MPO can be viewed as an MPS with physical dimension $d^2$, graphically shown in Fig. 3.7. MPS and MPO are thus generally defined as *matrix product vectors* (MPV) (Cirac et al., 2017). Note that there is a subtlety as to the distance minimized: in the MPS case, it is the Euclidean distance defined in Eq. (3.21), while for an MPO, it would be the Frobenius norm

$$\left|\left|\hat{A}\right|\right|_F^2 := \mathrm{tr}\left(\hat{A}\hat{A}^\dagger\right), \tag{3.28}$$

where $\hat{A} = \hat{O}^{(D)} - \hat{\tilde{O}}^{(\tilde{D})}$.

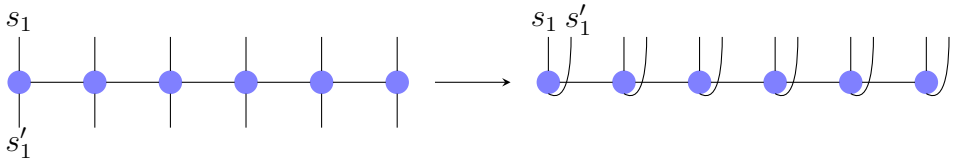


Figure 3.7: MPO viewed as MPS with double physical indices.

An MPO can be used to efficiently represent or approximate those operators satisfying area laws, in particular local Hamiltonians (McCulloch, 2007; Pirvu et al., 2010), Gibbs states (Molnar et al., 2015; Verstraete et al., 2004a) and short time evolution operators (Vidal, 2004). The last two will be discussed in section 3.4.2.

**MPO exact representation of local Hamiltonians (McCulloch, 2007; Pirvu et al., 2010).** Consider the nearest neighbor interacting Hamilto-

nian

$$\hat{H} = \sum_{n=1}^{N-1} \hat{X}_n \hat{Y}_{n+1} + \sum_{n=1}^{N} \hat{Z}_n. \tag{3.29}$$

The matrices can be chosen as

$$M_1^{s_1,s_1'} = \begin{pmatrix} \hat{Z}_1^{s_1,s_1'} & \hat{X}_1^{s_1,s_1'} & \mathbb{1}^{s_1,s_1'} \end{pmatrix}, \quad M_N^{s_N,s_N'} = \begin{pmatrix} \mathbb{1}^{s_N,s_N'} \\ \hat{Y}_N^{s_N,s_N'} \\ \hat{Z}_N^{s_N,s_N'} \end{pmatrix} \tag{3.30}$$

and

$$M_n^{s_n,s_n'} = \begin{pmatrix} \mathbb{1}^{s_n,s_n'} & 0 & 0 \\ \hat{Y}_n^{s_n,s_n'} & 0 & 0 \\ \hat{Z}_n^{s_n,s_n'} & \hat{X}_n^{s_n,s_n'} & \mathbb{1}^{s_n,s_n'} \end{pmatrix} \tag{3.31}$$

for $1 < n < N$. From the construction, it can be observed that the total bond dimension required is $2 + \sum_k (r_k - 1)$, where $r_k$ is the acting range of each term of interactions.

## 3.4 Algorithms

Two MPS/MPO-based algorithms of most significance will be covered in this section: variational search of ground states and (real and imaginary) time evolution algorithms.

### 3.4.1 Variational search of ground states

As discussed in section 3.2.2, small-eigenvalue subspaces of the reduced density matrices of an MPS can be truncated to obtain smaller bond dimensions. This is the spirit of the approximation in the density matrix renormalization group (DMRG) algorithm, used to find ground states. In the language of tensor networks, we aim to find an MPS $|\psi^{(D)}\rangle$ with bond dimension $D$ to minimize the energy $E = \langle\psi^{(D)}|\hat{H}|\psi^{(D)}\rangle \,/\, \langle\psi^{(D)}|\psi^{(D)}\rangle$.

Consider the conditions of a extremal point $\boldsymbol{x}_0$ of $\lambda(\boldsymbol{x}) = f(\boldsymbol{x})/g(\boldsymbol{x})$, where $\boldsymbol{x} = (x_1, \cdots, x_L)$, $g(\boldsymbol{x}) > 0$ and $f(\boldsymbol{x}_0)/g(\boldsymbol{x}_0) =: \lambda_0$:

$$\frac{\partial}{\partial x^i}\left(\frac{f}{g}\right)(\boldsymbol{x}_0) = 0 \Rightarrow \frac{\partial}{\partial x^i} f(\boldsymbol{x}_0) = \lambda_0 \frac{\partial}{\partial x^i} g(\boldsymbol{x}_0). \tag{3.32}$$

In our problem, for an MPS $|\psi^{(D)}\rangle = \sum_{\boldsymbol{s}} \mathrm{tr}\left(M_1^{s_1}\cdots M_N^{s_N}\right)|\boldsymbol{s}\rangle$ with OBC it becomes

$$\frac{\partial \langle\psi^{(D)}|\hat{H}|\psi^{(D)}\rangle}{\partial\left(M_n^{s_n'*}\right)_{a_{n-1}'a_n'}} = E_0^{(D)}\frac{\partial \langle\psi^{(D)}|\psi^{(D)}\rangle}{\partial\left(M_n^{s_n'*}\right)_{a_{n-1}'a_n'}}, \tag{3.33}$$

which can be graphically represented as

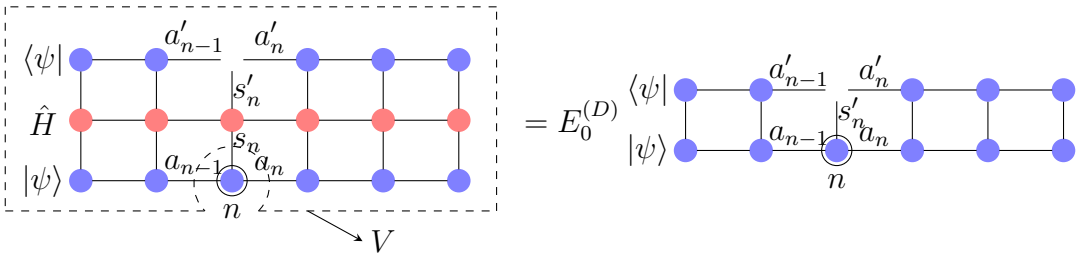


(3.34)

for each site $n$. It is an $dD^2\times dD^2$-dimensional generalized eigenvalue problem for $(M_n^{s_n})_{a_{n-1}a_n}$:

$$\begin{aligned} &V_{(a_{n-1}'a_n's_n'),(a_{n-1}a_ns_n)}(M_n^{s_n})_{a_{n-1}a_n} \\ =&E_0^{(D)}N_{(a_{n-1}'a_n'),(a_{n-1}a_n)}\delta_{s_n,s_n'}(M_n^{s_n})_{a_{n-1}a_n}. \end{aligned} \tag{3.35}$$

Again, when the MPS is in mixed-canonical form centered at site $n$, $N$ is an identity matrix and the equation is reduced to

$$V_{(a_{n-1}'a_n's_n'),(a_{n-1}a_ns_n)}(M_n^{s_n})_{a_{n-1}a_n} = E_0^{(D)}(M_n^{s_n'})_{a_{n-1}'a_n'}. \tag{3.36}$$

The same algorithm as the truncation of MPS can be applied, while in each step of the sweep, one has to solve the smallest eigenvalue of Eq. (3.36) as the current minimum energy and update $M_n$ with the corresponding eigenstate. As there is no need to diagonalize the whole matrix, the Lanczos algorithm is sufficient. Its speed of convergence depends greatly on the initial guess state. The current matrices $M_n$ will be a good choice, which dramatically speeds up the solver (Schollwöck, 2011). The contractions are now more complicated due to the involvement of MPO $\hat{H}^{(D_o)}$, which ends up in time complexity $\mathcal{O}(dD_oD^3 + d^2D_o^2D^2)$.

This algorithm can be extended to low lying excited states as well, if we project the Hamiltonian onto the subspace orthogonal to the lower lying

states, after having obtained all of them (Bañuls et al., 2013):

$$\hat{H}' = \hat{H} - \sum_{k=0}^{l} E_k \left|k\right\rangle \left\langle k\right| \approx \hat{H}^{(D_o)} - \sum_{k=0}^{l} E_k \left|k^{(D)}\right\rangle \left\langle k^{(D)}\right|. \tag{3.37}$$

The extra terms lead to a total leading time cost $\mathcal{O}(l^2 dD^3)$ if we want to find $l$ lowest lying states.

### 3.4.2 Real and imaginary time evolutions

**Time-evolving block decimation (TEBD) algorithm (Vidal, 2004).** Consider a nearest neighbor interacting Hamiltonian

$$\hat{H} = \sum_{n=1}^{N-1} \hat{h}_{n,n+1}. \tag{3.38}$$

In general an exact representation of the time evolution operator $\hat{U}_{\hat{H}}(t) = e^{-i\hat{H}t}$ is difficult with an MPO, since the local Hamiltonians do not commute with the neighboring terms and $\hat{U}_{\hat{H}}(t)$ is not separable. It is however possible to select commuting terms, for instance those start only from even or odd sites:

$$\hat{H} = \sum_{n \text{ even}} \hat{h}_{n,n+1} + \sum_{n \text{ odd}} \hat{h}_{n,n+1} =: \hat{H}_e + \hat{H}_o. \tag{3.39}$$

As $\hat{h}_{n,n+1}$ takes only a small Hilbert space dimension $d^2$, $e^{-i\hat{h}_{n,n+1}}$ and thus $\hat{U}_{\hat{H}_e}(t) = \prod_{n \text{ even}} \hat{U}_{\hat{h}_{n,n+1}}(t)$ (or $U_{\hat{H}_o}(t)$) can be exactly written down.

The Suzuki-Trotter expansions (Hatano and Suzuki, 2005) for this two non-commuting groups can then apply, which reads in the $p$-th order

$$e^{\delta(\hat{A}+\hat{B})} = f_p(e^{\delta\hat{A}}, e^{\delta\hat{B}}) + \mathcal{O}(\delta^{p+1}). \tag{3.40}$$

In the first order, $f_1(x, y) = xy$ while in the second, $f_2(x, y) = x^{1/2} y x^{1/2}$. The error can be well controlled for small enough time steps $\delta = t/M$, where $M \in \mathbb{N}$. The evolution operator can then be approximated as

$$\begin{aligned} \hat{U}_{\hat{H}}(t) &= \hat{U}_{\hat{H}}(\delta)^M \\ &= \left(f_p\left(\hat{U}_{\hat{H}_e}(\delta), \hat{U}_{\hat{H}_o}(\delta)\right) + \mathcal{O}(\delta^{p+1})\right)^N \\ &= \left(f_p\left(\hat{U}_{\hat{H}_e}(\delta), \hat{U}_{\hat{H}_o}(\delta)\right)\right)^M + \mathcal{O}(\delta^p t). \end{aligned} \tag{3.41}$$

The time evolution of an initial MPS $|\psi^{(D)}\rangle$ can be done by successively applying the $(p+1)M$ evolution operators of even or odd sites and truncating the resulting MPS to the preset bond dimension $D$. For each gate $\hat{O}_n := e^{i\hat{h}_{n,n+1}\delta}$, only a local update of two tensors is required if the MPS is kept in $\Gamma\Lambda$-notation

$$|\psi^{(D)}\rangle = \sum_{\boldsymbol{s}} \Gamma_1^{s_1}\Lambda^{(1)}\Gamma_2^{s_2}\Lambda^{(2)}\cdots\Lambda^{(N-1)}\Gamma_N^{s_N}\,|\boldsymbol{s}\rangle\,, \tag{3.42}$$

where $\Gamma_n^{s_n}\Lambda^{(n)} = B_n^{s_n}$ satisfies the right normalization condition, and we are taking the singular values out. We do not store the $\Gamma$ matrices, but only $B$ matrices and singular values $\Lambda^{(n)}$. Applying $\hat{O}_n$ results in

$$\begin{aligned}\left(B_n^{s_n}B_{n+1}^{s_{n+1}}\right)_{a_{n-1},a_{n+1}} &\to \sum_{s_n',s_{n+1}'} O_n^{s_n',s_{n+1}'}\left(B_n^{s_n}B_{n+1}^{s_{n+1}}\right)_{a_{n-1},a_{n+1}} \\ &=: \Phi^{s_n,s_{n+1}}_{a_{n-1},a_{n+1}}.\end{aligned} \tag{3.43}$$

We can carry out SVD on $\Lambda^{(n-1)}\Phi^{s_n,s_{n+1}}_{a_{n-1},a_{n+1}}$ and truncate it down to the $D$ largest singular values:

$$\begin{aligned}\Lambda^{(n-1)}\Phi^{s_n,s_{n+1}}_{a_{n-1},a_{n+1}} &\approx \sum_{a_n=1}^{D} U_{(a_{n-1}s_n),a_n}\tilde{\Lambda}^{(n)}_{a_n,a_n}V^{\dagger}_{a_n,(a_{n+1}s_{n+1})} \\ &=: \left(\tilde{A}_n^{s_n}\right)_{a_{n-1},a_n}\tilde{\Lambda}^{(n)}\left(\tilde{B}_{n+1}^{s_{n+1}}\right)_{a_n,a_{n+1}}.\end{aligned} \tag{3.44}$$

Finally, update the following matrices:

$$\begin{aligned}\Lambda^{(n)} &\leftarrow \tilde{\Lambda}^{(n)} \\ B_{n+1}^{s_{n+1}} &\leftarrow \tilde{B}_{n+1}^{s_{n+1}} \\ B_n^{s_n} &\leftarrow \sum_{s_{n+1}} \Phi^{s_n,s_{n+1}}\tilde{B}_{n+1}^{s_{n+1}\dagger}.\end{aligned} \tag{3.45}$$

This algorithm is named *time-evolving block decimation* (TEBD). Alternatively, the total time evolution operator $\hat{U}_{\hat{H}}(t)$ can also be approximated by an MPO. There are two main sources of errors. One is introduced by the Suzuki-Trotter expansion, which is of order $\mathcal{O}(\delta^p t)$ for a $p$-th order expansion. The other is the truncation error, which means the maximum time that TEBD can reach is limited by the entanglement entropy. Following

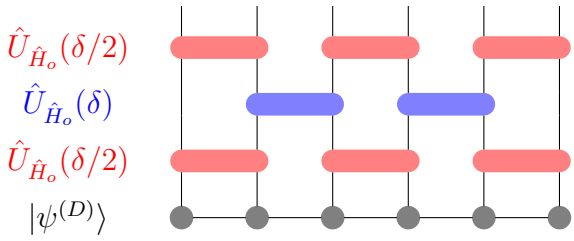


Figure 3.8: Time-evolving block decimation.

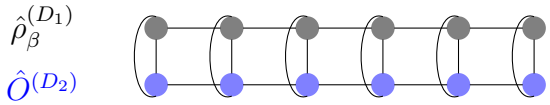


Figure 3.9: Gibbs state expectations

the Lieb-Robinson bounds (Calabrese and Cardy, 2005; Lieb and Robinson, 1972), it grows in some cases as $S(t) \leq S(t=0) + ct$ for some constant $c$ characterizing the speed of entanglement spreads. This indicates an exponentially increasing demand of bond dimensions, $D \sim \mathcal{O}(e^t)$, or inversely, for a fixed bond dimension, the error grows exponentially with time.

**Matrix product density operators for Gibbs states.** Let us now switch from real time to imaginary time $t = -i\beta$. The evolution operators correspond to the Gibbs states, or canonical ensemble density operators

$$\hat{\rho}_\beta = \frac{e^{-\beta\hat{H}}}{\mathrm{tr}\left(e^{-\beta\hat{H}}\right)}. \tag{3.46}$$

MPO are, in contrast to the case of real time evolution operators, good representations of $\hat{\rho}_\beta$ at any finite temperature for local Hamiltonians (Kuwahara et al., 2021; Molnar et al., 2015). The ensemble expectation of the observable $\hat{O}$ as an MPO can therefore be efficiently calculated by $\bar{O}_{\mathrm{Gibbs},\beta} = \mathrm{tr}\left(\hat{O}\hat{\rho}_\beta\right)$.

# Chapter 4

# Spectral Analysis with Kernel Polynomial Method

In this chapter, we introduce *the kernel polynomial method (KPM)* (Weiße et al., 2006), which allows access to spectral and thus dynamical properties by iterative operator multiplications. As an alternative to exact diagonalization method, no explicit eigenstate decomposition is required. Combined with TNS, the KPM can be applied to quantum many body systems for spectral analysis (Halimeh et al., 2015; Holzner et al., 2011; Wolf et al., 2015; Xie et al., 2017; Yang et al., 2020). In particular, we use it to compute the GDOS, which can approximate microcanonical ensemble expectations and probe quantum thermalization through its difference from Gibbs ensemble values (Yang et al., 2020).

## 4.1 Chebyshev expansion and the kernel polynomial method

The basic idea of KPM is to approximate the desired functions by its expansion in an orthogonal polynomial basis of the appropriate Sobolev space. In general all such orthogonal polynomial basis can be used, while the (kernel) Chebyshev polynomials, as the best polynomial approximation for functions in $L^2(-1,1)$, prove to be the best choice for most applications. Below we present a quick review on KPM based on Weiße et al. (2006).

### 4.1.1 Definition of Chebyshev polynomials

We define first two types of inner products for $f, g \in L^2(-1,1)$:

$$\begin{aligned}\langle f|g\rangle_1 &= \int_{-1}^{1} w_1(x) f(x) g(x) \mathrm{d}x = \int_{-1}^{1} \frac{f(x)g(x)}{\pi\sqrt{1-x^2}} \mathrm{d}x, \\ \langle f|g\rangle_2 &= \int_{-1}^{1} w_2(x) f(x) g(x) \mathrm{d}x = \int_{-1}^{1} \pi\sqrt{1-x^2} f(x)g(x) \mathrm{d}x.\end{aligned} \tag{4.1}$$

They give rise to the two kinds of Chebyshev polynomials $T_n(x)$ and $U_n(x)$, with corresponding orthogonal relations

$$\begin{aligned} T_n(x) &= \cos(n \arccos(x)), & \langle T_n|T_m\rangle_1 &= \frac{1+\delta_{n,0}}{2}\delta_{n,m}; \\ U_n(x) &= \frac{\sin((n+1)\arccos(x))}{\sin(\arccos(x))}, & \langle U_n|U_m\rangle_2 &= \frac{\pi^2}{2}\delta_{n,m}. \end{aligned} \tag{4.2}$$

Eq. (4.2) can be rewritten recursively in the form of polynomials:

$$\begin{aligned} &T_0(x) = 1, \quad T_1(x) = x, \quad T_{n+1}(x) = 2xT_n(x) - T_{n-1}(x), \ n \geq 1; \\ &U_0(x) = 1, \quad U_1(x) = 2x, \quad U_{n+1}(x) = 2xU_n(x) - U_{n-1}(x), \ n \geq 1. \end{aligned} \tag{4.3}$$

From the definition of Chebyshev polynomials, the properties of sine and cosine functions can be used to write the identities that will be used later:

$$\begin{aligned} 2T_m(x)T_n(x) &= 2\cos(m\arccos(x))\cos(n\arccos(x)) \\ &= \cos((m+n)\arccos(x)) + \cos((m-n)\arccos(x)) \\ &= T_{m+n}(x) + T_{|m-n|}(x), \end{aligned} \tag{4.4}$$

$$\begin{aligned} 2U_{m-1}(x)U_{n-1}(x) &= \frac{2\sin(m\arccos(x))\sin(n\arccos(x))}{\sin(\arccos(x))^2} \\ &= \frac{\cos((m-n)\arccos(x)) - \cos((m+n)\arccos(x))}{1-x^2} \\ &= \frac{T_{|m-n|}(x) - T_{m+n}(x)}{1-x^2}. \end{aligned} \tag{4.5}$$

The standard way of expanding a function $f \in L^2(-1,1)$ in terms of Chebyshev polynomials (of the first kind for instance) is thus

$$f(x) = \sum_{n=0}^{\infty} \frac{\langle f|T_n\rangle_1}{\langle T_n|T_n\rangle_1} T_n(x). \tag{4.6}$$

It will however involve integrals with weights $w_1(x) = 1/\pi\sqrt{1-x^2}$. A trick to avoid it is to use the modified functions

$$\phi_n(x) = \frac{T_n(x)}{\pi\sqrt{1-x^2}} \tag{4.7}$$

whose orthogonal relations read

$$\langle\phi_n|\phi_m\rangle_2 = \frac{1+\delta_{n,0}}{2}\delta_{n,m}. \tag{4.8}$$

The resulting expansion of $\phi_n(x)$ is

$$\begin{aligned} f(x) &= \sum_{n=0}^{\infty} \frac{\langle f|\phi_n\rangle_2}{\langle\phi_n|\phi_n\rangle_2} T_n(x) \\ &= \frac{1}{\pi\sqrt{1-x^2}}\left[\mu_0 + 2\sum_{n=1}^{\infty}\mu_n T_n(x)\right], \end{aligned} \tag{4.9}$$

where

$$\mu_n = \langle f|\phi_n\rangle_2 = \int_{-1}^{1} f(x)T_n(x)\mathrm{d}x. \tag{4.10}$$

### 4.1.2 Gibbs oscillation and kernels

So far we discussed only the infinite series. In practical calculation, we can only expand up to finite terms

$$f(x) \approx f_M(x) = \frac{1}{\pi\sqrt{1-x^2}}\left[\mu_0 + 2\sum_{n=1}^{M-1}\mu_n T_n(x)\right]. \tag{4.11}$$

It is proved that Eq. (4.11) is a good approximation for functions in the standard Sobolev spaces $H^l(-1,1)$ with $l \geq 2$ (Canuto and Quarteroni, 1982) that uniformly converges as $M \to \infty$. If $f$ is not continuously differentiable at some points, however, this finite sum leads to large fluctuations, also called *Gibbs oscillations*. Our goal is to find the best uniform approximation, i.e., to minimize $||f - f_M||_\infty$ by adapting the moments $\mu_n \to \gamma_n\mu_n$, where the coefficients $\gamma_n$ are independent of $x$. This problem has been studied for at least 150 years and many known mathematicians including Chebyshev, Weierstrass, Dirichlet, Fejér and Jackson provided fruitful results.

The modified expansion can be reformulated to be the convolution of $f(x)$ with the *kernel* $K_N(x,y)$:

$$\begin{aligned} K_M(x,y) &= \gamma_0\phi_0(x)\phi_0(y) + 2\sum_{n=1}^{M-1}\gamma_n\phi_n(x)\phi_n(y), \\ f_M^{\mathrm{KPM}} &= \langle K_M(x,y)|f(y)\rangle_2 . \end{aligned} \tag{4.12}$$

The problem is translated to find the optimal kernel. The trivial case is the Dirichlet kernel with $\gamma_n^D = 1$ and

$$\begin{aligned} K_M^D &= \phi_0(x)\phi_0(y) + 2\sum_{n=1}^{M-1}\phi_n(x)\phi_n(y) \\ &= \frac{\phi_M(x)\phi_{M-1}(y) - \phi_{M-1}(x)\phi_M(y)}{x-y}. \end{aligned} \tag{4.13}$$

Especially in our applications to generalized DOS, the kernel should be positive ($K_N(x,y) \geq 0 \forall x,y \in (-1,1)$) and normalized ($\int_{-1}^{1} K(x,y)\mathrm{d}x = \phi_0(y)$).

The first improvement is achieved by Fejér (Fejér, 1903):

$$\gamma_n^F = 1 - \frac{n}{M}. \tag{4.14}$$

We will not discuss the detailed derivations, which can be found in (Weiße et al., 2006). This kernel gives uniform convergence in a restricted interval $[-1+\epsilon, 1-\epsilon]$ for any $0 < \epsilon < 1$. It can be further shown that

$$\left|\left|f - f_M^F\right|\right|_\infty^\epsilon \sim w_f\left(\frac{1}{\sqrt{M}}\right), \tag{4.15}$$

where

$$w_f(\Delta) := \max_{|x-y|\leq\Delta} |f(x) - f(y)| . \tag{4.16}$$

Jackson (Jackson, 1911) later proposed a better version

$$\gamma_n^J = \frac{(M-n+1)\cos\frac{\pi n}{M+1} + \sin\frac{\pi n}{M+1}\cot\frac{\pi}{M+1}}{M+1} \tag{4.17}$$

which reduces the error with factor $1/\sqrt{M}$ (for continuous functions)

$$\left|\left|f - f_M^J\right|\right|_\infty^\epsilon \sim w_f\left(\frac{1}{M}\right). \tag{4.18}$$

Another kernel often employed in the calculation of Green's functions is the Lorentz kernel, which preserves the causality:

$$\gamma^L_{n,\lambda} = \frac{\sinh\left[\lambda(1-\frac{n}{N})\right]}{\sinh\lambda}, \tag{4.19}$$

where $\lambda$ is a real parameter.

For most physical applications, *the Jackson kernel* is the optimal choice (Weiße et al., 2006). In the following, $f_M$ denotes $f_M^{\mathrm{KPM}}$ using the Jackson kernel without any specification.

### 4.1.3 Chebyshev expansions of Dirac-$\delta$ and Heaviside step functions

Here we explicitly show the Chebyshev expansion for two special functions that are especially relevant to our work.

**Dirac-$\delta$ function.** Consider $f(x) = \delta(x-a)$ being the Dirac-$\delta$ function centered at $a \in (-1,1)$. It follows that $\mu_n = \int_{-1}^{1} \delta(x-a)T_n(x) = T_n(a)$ and hence

$$\delta_M(x-a) = \frac{1}{\pi\sqrt{1-x^2}}\left[\gamma_0 T_0(a) + 2\sum_{n=1}^{M-1}\gamma_n T_n(a)T_n(x)\right]. \tag{4.20}$$

The $\delta$ function is broadened by a finite expansion, which can be characterized by its variance if we consider $\delta_M(x-a)$ to be a probability distribution. Using $x = T_1(x)$ and $x^2 = [T_0(x)+T_2(x)]/2$, it is easy to compute

$$\begin{aligned}\langle x\rangle &= \int_{-1}^{1} T_1(x)\delta_M(x-a) \\ &= \gamma_0 T_0(a)\left\langle T_1|T_0\right\rangle_1 + 2\sum_{n=1}^{M-1}\gamma_n T_n(a)\left\langle T_1|T_n\right\rangle_1 = \gamma_1 T_1(a), \\ \langle x^2\rangle &= \int_{-1}^{1}\frac{T_0(x)+T_2(x)}{2}\delta_M(x-a) = \frac{\gamma_0 T_0(a)+\gamma_2 T_2(a)}{2}.\end{aligned} \tag{4.21}$$

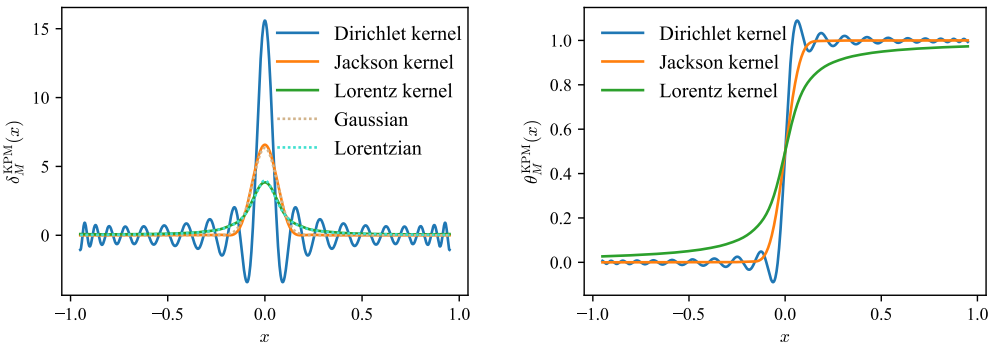


Figure 4.1: $\delta_M(x)$ (left) and $\theta_M(x)$ (right) using different kernels with $M = 50$. $\lambda = 4$ for the Lorentz kernel. The width of Gaussian and Lorentzian are $\pi/M$ and $\lambda/M$ respectively.

Therefore the variance is given by

$$\begin{aligned}\sigma^2 &= \langle x^2 \rangle - \langle x \rangle^2 \\ &= \frac{M - a^2(M-1)}{2(M+1)} \left(1 - \cos\frac{2\pi}{M+1}\right) \\ &\simeq \left(\frac{\pi}{M}\right)^2 \left[1 - a^2 + \frac{3a^2 - 2}{M}\right]\end{aligned} \tag{4.22}$$

for large $M$. When $a = 0$, $\sigma = \pi/M$ and $\delta_M(x)$ proves to be close to a Gaussian

$$\delta_M(x) \approx \frac{1}{\sqrt{2\pi}\sigma} e^{-\frac{x^2}{2\sigma^2}}. \tag{4.23}$$

**Heaviside step function.** Consider $f(x) = \theta(x - a)$ being the Heaviside step function such that

$$\theta(x-a) = \begin{cases} 0, & x < a; \\ 1, & x \geq a. \end{cases} \tag{4.24}$$

In this case, we can take back the standard expansion, for the integral with weight $w_1(x)$ can be calculated exactly:

$$\alpha_n^\theta := \int_{-1}^{1} \frac{\theta(x-a)T_n(x)}{\pi\sqrt{1-x^2}} = \begin{cases} \dfrac{\arccos a}{\pi}, & n=0; \\ \dfrac{\sin(n\arccos a)}{n\pi}, & n \geq 1 \end{cases} \tag{4.25}$$

and

$$\theta_M(x-a) = \gamma_0\alpha_0^\theta + 2\sum_{n=1}^{M-1}\gamma_n\alpha_n^\theta T_n(x). \tag{4.26}$$

## 4.2 Spectral analysis by KPM combined with TNS

Based on the materials discussed above, in Yang et al. (2020) we applied KPM to approximate the GDOS. Recall their definition in Eq. (2.8):

$$g(E,\hat{O}) = \mathrm{tr}\left[\hat{O}\delta(E-\hat{H})\right]. \tag{4.27}$$

In order to perform the Chebyshev expansion, we should first rescale the Hamiltonian $\hat{H}$ such that its spectrum lies in the interval $[-1+\epsilon, 1-\epsilon]$ for some small constant $\epsilon$. The rescaled the Hamiltonian is denoted by $\tilde{H} = \hat{H}/\nu + \Delta E$. Also let $\tilde{E} = E/\nu + \Delta E$. Then

$$\begin{aligned} g(E,\hat{O}) &= \frac{1}{\nu}\mathrm{tr}\left[\hat{O}\delta(\tilde{E}-\tilde{H})\right] \\ \approx & g_M(E,\hat{O}) := \frac{1}{\nu}\cdot\frac{1}{\pi\sqrt{1-\tilde{E}^2}}\left[g_0\mu_0 + 2\sum_{n=1}^{M-1} g_n\mu_n T_n(\tilde{E})\right], \end{aligned} \tag{4.28}$$

where the corresponding Chebyshev moments are

$$\mu_n(\tilde{H},\hat{O}) = \mathrm{tr}\left[\hat{O}T_n(\tilde{H})\right]. \tag{4.29}$$

In general, $T_n(\tilde{H})$ can be calculated iteratively using MPO, while for the LDOS case, more efficient calculations are allowed.

### 4.2.1 LDOS-like case

Consider $\hat{O} = |\psi\rangle\langle\phi|$ that projects a single state to another. Other than LDOS, this form of $\hat{O}$ can as well represent the *zero-temperature spectral functions* (Holzner et al., 2011; Wolf et al., 2015; Xie et al., 2017)

$$\mathcal{A}^{BC}(\omega) = \langle 0|\hat{B}\delta(\omega - \hat{H} + E_0)\hat{C}|0\rangle \tag{4.30}$$

which is the Fourier transform of the ground state correlator

$$G^{BC} = \langle 0|\hat{B}(t)\hat{C}(0)|0\rangle\,. \tag{4.31}$$

The spectral function can be experimentally detected, for instance by angle-resolved photoemission spectroscopy (ARPES).

The corresponding Chebyshev moments are

$$\mu_n(\tilde{H}, \hat{O}) = \langle\phi|T_n(\tilde{H})|\psi\rangle\,. \tag{4.32}$$

When $|\psi\rangle$ and $|\phi\rangle$ have efficient MPS representations, Eq. (4.32) can also be efficiently computed. Let $|t_0^{(D)}\rangle = |\psi^{(D)}\rangle$, $|t_1^{(D)}\rangle \approx \tilde{H}\,|t_0\rangle$ and the the recurrence relation reads

$$|t_n^{(D)}\rangle \approx 2\tilde{H}\,|t_{n-1}^{(D)}\rangle - |t_{n-1}^{(D)}\rangle\,,\ n \geq 2. \tag{4.33}$$

The right hand side can be viewed as the sum of two MPS, so that the compression algorithm in section 3.2.2 can be applied to approximate $T_n(\tilde{H})\,|\psi\rangle$ with an MPS $|t_n^{(D)}\rangle$ of bond dimension $D$. Finally $\mu_n^{(D)} = \langle\phi^{(D)}|t_n^{(D)}\rangle$. This procedure is similar to the Lanczos recursion method (see details in (Weiße et al., 2006)), but avoids the problem of vectors losing orthogonality and has better controlled resolution $\propto 1/M$.

### 4.2.2 DOS-like case

In the general case with a trace in Eq. (4.29), we need to keep the full $T_n(\tilde{H})$ operator approximated by an MPO $T_n(\tilde{H})^{(D)}$ using the recursive relation

$$T_n^{(D)}(\hat{H}) \approx 2\tilde{H}T_{n-1}^{(D)}(\tilde{H}) - T_{n-2}^{(D)}(\tilde{H}) \tag{4.34}$$

and

$$\mu_n^{(D)}(\tilde{H}, \hat{O}) = \mathrm{tr}\left[\hat{O}T_n^{(D)}(\tilde{H})\right]. \tag{4.35}$$

When applied to calculate the microcanonical ensemble average

$$O_M(E) = \frac{g_M(E, \hat{O})}{g_M(E, \mathbb{1})}, \tag{4.36}$$

a direct division will not numerically provide correct numbers near the edge of the spectrum due to the exponentially decaying tail of DOS. For the short-range interacting case as discussed in section 2.2.1, the DOS scales as $\mathcal{O}(\exp(-E^2/\alpha^2 N)/\sqrt{N})$ compared with the peak. For large $N$, it could be smaller than machine precision.

This problem can be partially solved by projecting the Hamiltonian onto smaller energy intervals $\hat{H} \to \theta_R(\hat{H} - E_{\text{th}})\hat{H}$ (if we focus on the right end of spectrum without losing generality, see Fig. 4.2) with step operators expanded to the $R-$th term, also using KPM. It is equivalent to inserting $\theta_R(\tilde{H} - \tilde{E}_{\text{th}})$ to $\mu_n$:

$$\begin{aligned} \mu_n(\tilde{H}, \hat{O}) &\to \operatorname{tr}\left[\hat{O}T_n(\tilde{H})\theta_R(\tilde{H} - \tilde{E}_{\text{th}})\right] \\ &= \operatorname{tr}\left[\hat{O}T_n(\tilde{H})\left(\gamma_0^R\alpha_0^\theta + 2\sum_{m=1}^{R-1}\gamma_m^R\alpha_m^\theta T_m(\tilde{H})\right)\right]. \end{aligned} \tag{4.37}$$

In principle, Eq. (4.37) can be computed if we store all the polynomials $T_n(\hat{H})$. But it is possible to proceed in a more efficient way. Recall Eq. (4.4) and apply it twice:

$$\begin{aligned} T_n(x)T_m(x) &= \frac{T_{n+m}(x) + T_{|n-m|(x)}}{2} \\ &= \begin{cases} T_{\frac{n+m}{2}}(x)T_{\frac{n+m}{2}}(x) + \frac{1}{2}\left[T_{|n-m|}(x) - T_0(x)\right], & n+m \text{ even}; \\ T_{\frac{n+m+1}{2}}(x)T_{\frac{n+m-1}{2}}(x) + \frac{1}{2}\left[T_{|n-m|}(x) - T_1(x)\right], & n+m \text{ odd}. \end{cases} \end{aligned} \tag{4.38}$$

This expression can thus be calculated if we further store $\operatorname{tr}\left[\hat{O}T_n^{(D)}(\tilde{H})T_n^{(D)}(\tilde{H})\right]$ and $\operatorname{tr}\left[\hat{O}T_n^{(D)}(\tilde{H})T_{n-1}^{(D)}(\tilde{H})\right]$ up to the $\max(M, R)$-th term, or use original $\mu_n$ up to the $(M + R - 1)$-th term.

Let us now explain in detail how to implement this energy cutoff for estimating $g(E, \hat{O})$ on $[E_{\min}, E_{\max}]$, from the right side of the spectrum for

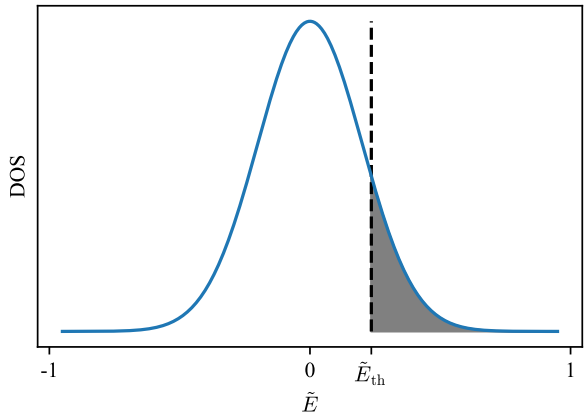


Figure 4.2: Cutting of DOS.

example:

**Algorithm 1:** Estimating $g_{M,R}(E, \mathbb{1})$ and $g_{M,R}(E, \hat{O})$ by cutting states off.

**init**
  Choose a reduction factor $\eta \in (0, 1)$ and a small safety parameter $\varepsilon$
  $s \leftarrow 0$, $E_s \leftarrow E_{\min}$
  Use Chebyshev expansions without a $\theta$ projector to provide an initial estimate $g_0(E, \mathbb{1})$ and $g_0(E, \hat{O})$ respectively for $g(E, \mathbb{1})$ and $g(E, \hat{O})$ in $[E_{\min}, E_{\max}]$
**while** $E_s < E_{max}$ **do**
  $E_{s+1} \leftarrow \sup \{ E \in [E_s, E_{\max}] \mid g_s(E_{s+1}; \mathbb{1}) \geq \eta g_s(E_s; \mathbb{1}) \}$
  $g_{M,R}([E_s, E_{s+1}], \mathbb{1}) \leftarrow g_s([E_s, E_{s+1}], \mathbb{1})$
  $g_{M,R}([E_s, E_{s+1}], \hat{O}) \leftarrow g_s([E_s, E_{s+1}], \hat{O})$
  Construct $g_{s+1}(E, \mathbb{1})$ and $g_{s+1}(E, \hat{O})$ from the moments $\mu_n(\tilde{H}, \theta_R(\tilde{H} - \tilde{E}_{s+1} - \varepsilon))$ and $\mu_n(\tilde{H}, \theta_R(\tilde{H} - \tilde{E}_{s+1} - \varepsilon)\hat{O})$
  $s \leftarrow s + 1$
**return** $g_{M,R}(E, \mathbb{1})$, $g_{M,R}(E, \hat{O})$

Denote the final estimates $O_{M,R}(E) = g_{M,R}(E, \hat{O})/g_{M,R}(E, \mathbb{1})$. This strategy does *not* actually introduce more information from the Hamilto-

nian, since the Chebyshev moments $\mu_n$ decay (exponentially) fast with $n$ and practically the higher terms whose indices exceed $M$ are negligible. It however *does* improve the estimate of GDOS near the edge of the spectrum, which will be illustrated in section 4.3.1. It works like a magnifying glass that focuses on the information local in some energy interval.

## 4.3 Applications

### 4.3.1 Ising model

We applied the method to two quantum spin chains with open boundary conditions. The first one is the Ising model, whose Hamiltonian is

$$\hat{H}_{\text{Ising}} = J \sum_{i=1}^{N-1} \hat{\sigma}_i^z \hat{\sigma}_{i+1}^z + g \sum_{i=1}^{N} \hat{\sigma}_i^x + h \sum_{i=1}^{N} \hat{\sigma}_i^z. \tag{4.39}$$

The Ising model is known to be non-integrable, except in the two limits $g \to 0$ (classical) and $h \to 0$ (transverse field Ising model). Non-trivial dynamics have been observed and investigated in the non-integrable regime (Bañuls et al., 2011; Hastings and Mahajan, 2015; James et al., 2019; Kormos et al., 2017; Lin and Motrunich, 2017) and in particular at the point $(J, g, h) = (1, -1.05, 0.5)$ that we use. An integrable point $(1, 0.8, 0)$ is also analyzed for comparison.

**DOS and LDOS.** In Fig. 4.3, the normalized DOS and LDOS of both non-integrable (left) and integrable (right) Ising models are plotted. For DOS, the well-behaved convergence with regard to expansion order $M$ can be observed, especially for the integrable case compared with exact result. Note that in this case, the Chebyshev moments $\mu_n$ are negligible when $n \gtrsim 100$, and this convergence is greatly due to the different kernel parameters $\gamma_n$ for different $M$. For LDOS, three translationally invariant product states $|X+\rangle = \left(\frac{|\uparrow\rangle+|\downarrow\rangle}{\sqrt{2}}\right)^{\otimes N}$, $|Y+\rangle = \left(\frac{|\uparrow\rangle+i|\downarrow\rangle}{\sqrt{2}}\right)^{\otimes N}$ and $|Z+\rangle = (|\uparrow\rangle)^{\otimes N}$ are considered. The shapes of both the DOS and the LDOS fit well with Gaussians as predicted in section 2.2.1, except for the LDOS near the edges.

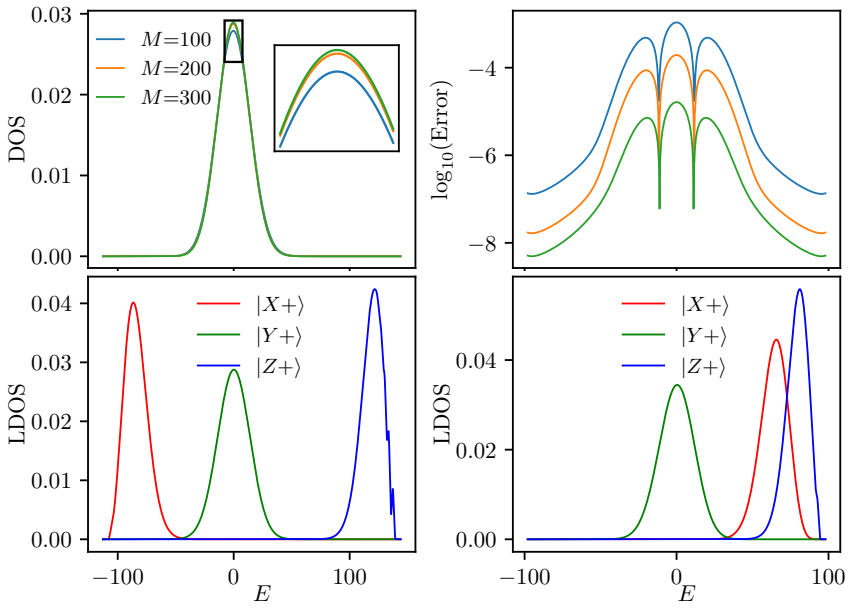


Figure 4.3: Normalized DOS ($g(E, \mathbb{1})/d_{\mathcal{H}}$, $d_{\mathcal{H}}$ being the dimension of Hilbert space; upper panel) and LDOS (lower panel) of Ising chains for system size $N = 80$. The left part is for the non-integrable parameter set and the right one is for the integrable case, which can be compared with the ED result. Bond dimension used is $D = 200$.

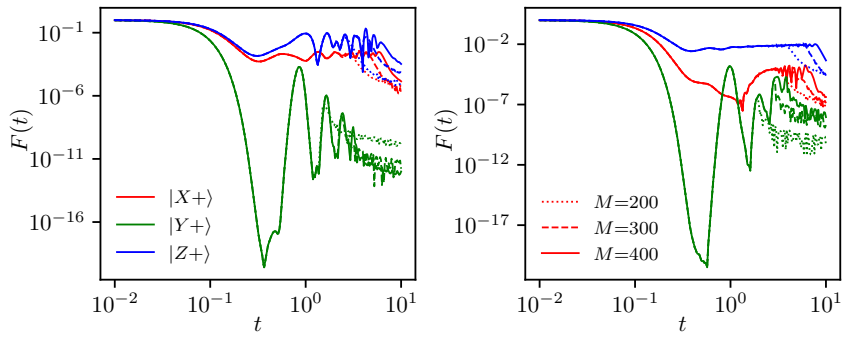


Figure 4.4: Survival probability of $|X+\rangle$, $|Y+\rangle$ and $|Z+\rangle$ of the non-integrable (left) and integrable (right) Ising models. System size $N = 40$. The different line styles corresponds to different truncation order of the LDOS.

**Loschmidt echo.** As discussed in section 2.2, the Loschmidt echo, or survival probability of state $|\psi\rangle$ is the Fourier transform of the LDOS:

$$F(t) = \left| \int g(E, |\psi\rangle \langle\psi|) e^{-iEt} \mathrm{d}E \right|^2 . \tag{4.40}$$

Due to the identity

$$\int_{-1}^{1} \frac{e^{ixt} T_n(x)}{\pi\sqrt{1-x^2}} \mathrm{d}x = i^n J_n(t), \tag{4.41}$$

its approximation using Chebyshev moments is equivalent to the expansion in Bessel functions of the first kind up to order $M$:

$$F_M(t) \approx \left| \frac{1}{\nu} \left[ \gamma_0 \mu_0 J_0(-\nu t) + 2 \sum_{n=1}^{M-1} i^n \gamma_n \mu_n J_n(-\nu t) \right] \right|^2 . \tag{4.42}$$

See Fig. 4.4 for the survival probability calculated this way. We point out that the Dirichlet kernel $\gamma_n = 1$ works the best in this situation, details in Appendix 6.2.

Though the maximum time we can reach is short (see the error analysis in section 4.3.3 and also (Halimeh et al., 2015)), we can already observe an algebraic decay of the revival peaks after the Gaussian decay in the $|Y+\rangle$ state of non-integrable Ising model, as predicted in Távora et al. (2016). The decay exponent $\gamma$ (such that $F(t) \propto t^{-\gamma}$) we obtained is around 8, which is however much larger than their expectation ($1 \leq \gamma \leq 2$). Further study can be carried out for this phenomenon.

**Thermalization probes.** As explained in section 2.2, we can probe thermalization of a given initial state by comparing its long time average and the corresponding thermal value, or that of the whole system by comparing the microcanonical values and thermal values.

In the non-integrable case, the observable we choose is the spin in the middle of the chain $\hat{O} = \hat{\sigma}^z_{N/2}$. In the integrable case, this operator vanishes for all energy eigenstates because of the symmetry and we instead consider $\hat{O} = \left(\sum_i \hat{\sigma}^z_i\right)^2$. In Fig. 4.5, we plotted as a function of $E$ the results of

- the Gibbs state expectation $\left(E(\beta), \bar{O}_{\mathrm{Gibbs},\beta}\right)$ (black dashed line), where

$$\bar{O}_{\mathrm{Gibbs},\beta} = \mathrm{tr}\left(\hat{O} e^{-\beta \hat{H}}\right) / \mathrm{tr}\left(e^{-\beta \hat{H}}\right) \tag{4.43}$$

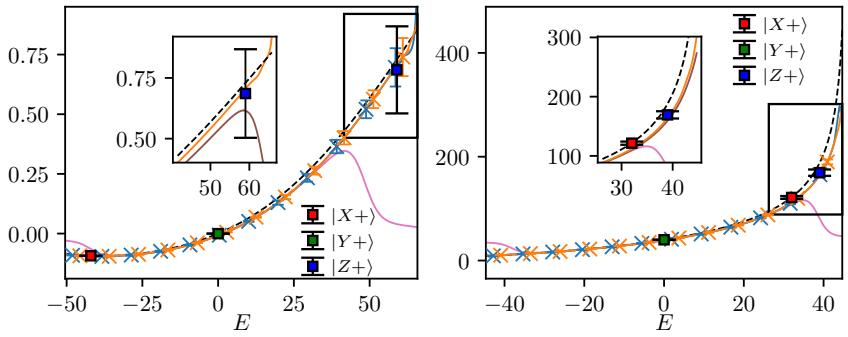


Figure 4.5: Thermalization probes for the non-integrable (left) and integrable (right) Ising models, for a chain of $N = 40$ sites. Dashed black line: Gibbs state expectation value of the corresponding observables. Orange line: $O_M(E)$ with $\theta$ projections; $M = 100$ (left), resp. $M = 150$ (right); $R = 100$; error bars indicate the difference with respect to truncation $M - 50$ (brown line in the inset); $D = 600$ (blue line for $D = 200$, with negligible error from bond dimension effect). Pink line: $O_M(E)$ of same $M$ without $\theta$ projections, failing for high energy regions. The red, green and blue points show the diagonal expectation values for the different initial states.

calculated by imaginary time TEBD algorithm and

$$E(\beta) = \mathrm{tr}\left(\hat{H}e^{-\beta\hat{H}}\right)/\mathrm{tr}\left(e^{-\beta\hat{H}}\right); \tag{4.44}$$

- bare thermalization probes $O_M(E)$ without $\theta$ projectors (pink line);
- thermalization probes $O_{M,R}(E)$ with $\theta$ projectors (orange line), where the error bars indicate the difference from $O_{M-50,R}$;
- same as the orange line, but with lower bond dimension (blue line);
- and the diagonal expectation value of different states $(\langle\psi|\hat{H}|\psi\rangle\,, O_{\mathrm{Diag}}(|\psi\rangle))$ (points), where

$$O_{\mathrm{Diag}}(|\psi\rangle) \approx \int O_{M,R}(E) g_{M'}(E,\psi)\mathrm{d}E. \tag{4.45}$$

See the caption of Fig. 4.5 for detailed parameters. Note that without the $\theta$ projector, $O_M(E)$ drops quickly in both edges, which is an effect of the

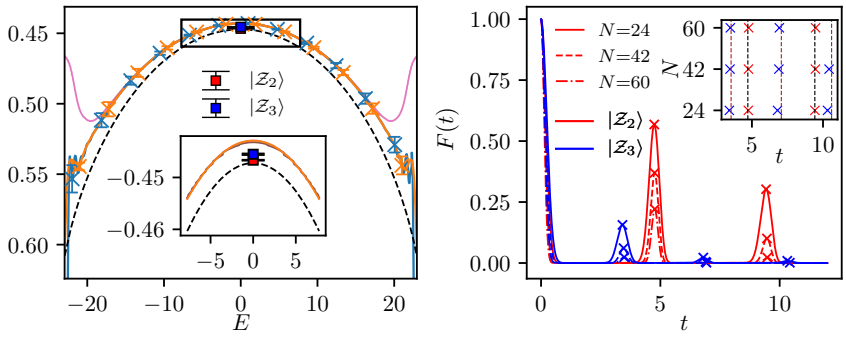


Figure 4.6: Thermalization probes for the PXP model. Left: the same quantities as Fig. 4.5 are plotted. Right: the survival probabilities of initial states $|\mathcal{Z}_2\rangle$ and $|\mathcal{Z}_3\rangle$.

enhanced error near the edges discussed above. The $\theta$ projector significantly improves the result.

As discussed in Eq. (2.22) in section 2.2.2, when ETH is fulfilled, the Gibbs and microcanonical values should coincide in the thermodynamic limit. In the non-integrable case, we observe convergence of $O_{M,R}(E)$ and $O_{\text{Diag}}(|\psi\rangle)$ to the Gibbs value $O_{\text{th}}(E)$ within the error bars. In the integrable case, however, we observe a deviation in the high energy region, which indicates non-thermal energy eigenstates there. The $|X+\rangle$ and $|Z+\rangle$ states of the non-integrable chain are particularly interesting, since numerical simulations are not able to reach the thermalization times for guaranteed consistency, while there are analytical arguments according to which the states should thermalize (Lin and Motrunich, 2017), which is compatible with our results. The large error bar for the $|Z+\rangle$ state comes from its closeness to the edge of the spectrum, which can be seen from its LDOS (lower-left plot of Fig. 4.3). In the integrable case, the most energetic state $|Z+\rangle$ does not satisfy the equilibrium condition. Nevertheless, it should be noted that for *degenerate* states, the diagonal ensemble average does *not* necessarily correspond to the long time limit.

### 4.3.2 PXP model

The PXP model is used to describe the dynamics of the Rydberg atom chain, in which the appearance of two consecutive excited atoms is forbidden (Bernien et al., 2017). Its Hamiltonian with open boundary conditions

is

$$\hat{H}_{\mathrm{PXP}} = \hat{\sigma}_1^x \hat{P}_2 + \sum_{i=2}^{N-1} \hat{P}_{i-1} \hat{\sigma}_i^x \hat{P}_{i+1} + \hat{P}_{N-1} \hat{\sigma}_N^x, \tag{4.46}$$

where $\hat{P}_i = (1 - \hat{\sigma}_i^z)/2$ is the projector to the ground state. It can be used to explain the Rydberg atoms where there are no neighboring excitation pairs by constraining the Hilbert space with the projector

$$\hat{P}_{\mathrm{Rydberg}} = \prod_{i=1}^{N-1} \left[ 1 - \left(1 - \hat{P}_i\right) \left(1 - \hat{P}_{i+1}\right) \right]. \tag{4.47}$$

The PXP model has been well investigated on the topic of quantum scars, a candidate mechanism to break quantum thermalization (Ho et al., 2019; Khemani et al., 2019; Lin, 2019; Turner et al., 2018a,b). The scar states form $N+1$ ETH-breaking towers, each containing $\mathcal{O}(N)$ states. The total number of these scars states is $\mathcal{O}(\mathrm{poly(N)})$, which is however much smaller than the Hilbert space dimension $d_N$ characterized by the Fibonacci number $F_{N+2}$ (visualized in Fig. 2 of (Turner et al., 2018a)). It breaks the condition of strong ETH, yet the weak form of ETH is still fulfilled since the ratio of scar states is negligible in the thermodynamic limit.

We have performed the same thermalization probe on the PXP model with the projected Hamiltonian $\hat{P}_{\mathrm{Rydberg}} \hat{H}_{\mathrm{PXP}} \hat{P}_{\mathrm{Rydberg}}$ and $\hat{O} = \hat{\sigma}_{N/2}^z$ and we show the results in Fig. 4.6. The Gibbs values and $O_{M,R}(E)$ agree the best in the middle of the spectrum, but the edges show larger deviations. This is compatible with the exact diagonalization result, that the ratio of scar states to ETH ones is the smallest in the middle of the spectrum due to the Gaussian shape of DOS.

The charge density wave states with periodicity $k$, $|\mathcal{Z}_k\rangle = |\underbrace{\uparrow\downarrow\downarrow\cdots\downarrow}_{k}\rangle^{\otimes N/k}$, are of particular interest in the PXP model. The spin up $|\uparrow\rangle$ and spin down $|\downarrow\rangle$ are the excited state and ground state of $\hat{\sigma}^z$ respectively. This class of periodic states, experimentally prepared by global quenches, are found to have unexpectedly long-lived oscillations in the Rydberg atoms (Bernien et al., 2017). We consider the simplest two of them, $|\mathcal{Z}_2\rangle$ and $|\mathcal{Z}_3\rangle$, as initial states. Their slow dynamics have been explained by their large overlaps with the scar states, which is enhanced when the system size is divisible by 6 (Turner et al., 2018a). Since the average energy of both states is 0, where there

is an exponentially large degeneracy, $O_{\text{Diag}}(|\mathcal{Z}_{2,3}\rangle)$ are not good estimates for the long time average (in the left figure of Fig. 4.6, they are compatible with the thermal value within error bars). Their survival probabilities from the LDOS, in contrast, present pronounced periodic revivals (right plot of Fig. 4.6). The periods are robust with regard to system size (see inset). These periods are theoretically $T_{\mathcal{Z}_2} \approx 3\pi/2$ and $T_{\mathcal{Z}_3} \approx 9\pi/8$ (Turner et al., 2018a). The height of the peaks, however, decreases (exponentially) with increasing $N$. This decline indicates that statistically, the non-thermal effects of scar states on general product states is weakened as the system enlarges, and possibly vanishes in the thermodynamic limit.

### 4.3.3 Error analysis

The errors of this method come from two distinct sources. The first one is the finite order cutoff of the Chebyshev expansion. As discussed in Eq. (4.18), for a continuous function $f \in L^2(-1,1)$, the finite sum of the first $M$ terms $f_M$ will converge uniformly to $f$ as

$$||f - f_M||_\infty \sim \mathcal{O}(1/M). \tag{4.48}$$

For small spin systems, increasing $M$ will eventually reveal the discrete nature of the spectrum at this point, the error scaling Eq. (4.48) is not valid any more. When we deal with large systems, such situation will not occur since the expansion width of each $\delta$ function is much larger than the level spacings, for the expansion order we can reach. The DOS in turn always look like smooth functions.

The second source is the bond dimension truncation when applying the recurrence condition. In order to estimate this error, we compute the Frobenius distance between the best applicable approximation $T_n^{(D_0)}(\tilde{H})$ (for the DOS-like case) with bond dimension $D_0$ and its truncations to $D < D_0$:

$$\epsilon_n(D) = \frac{\left|\left|T_n^{(D_0)}(\tilde{H}) - T_n^{(D)}(\tilde{H})\right|\right|_F^2}{\left|\left|T_n^{(D_0)}(\tilde{H})\right|\right|_F^2}. \tag{4.49}$$

For the LDOS-like case, we can analogously write for the state instead of the

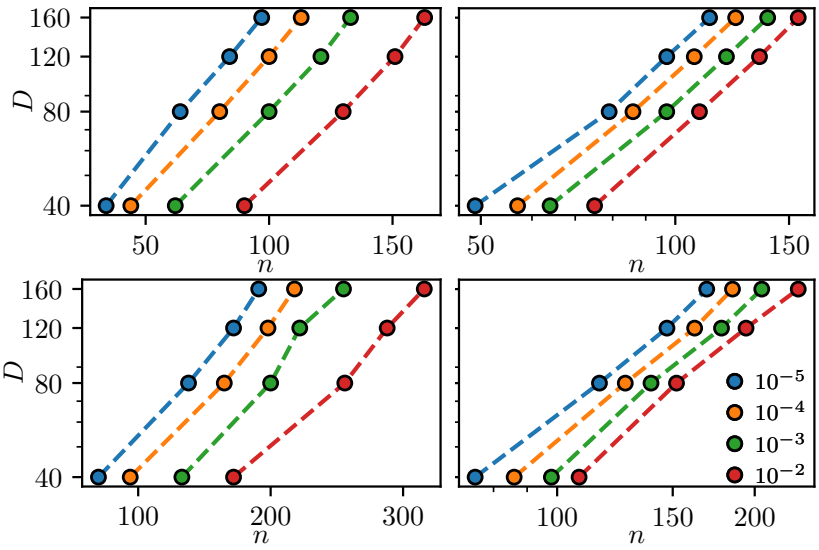


Figure 4.7: Bond dimension $D$ required to keep a given truncation error of $10^{-2}$, $10^{-3}$, $10^{-4}$ and $10^{-5}$. $D_0 = 200$. The left panel is a semi-log plot of $\epsilon_n(D)$ of the DOS-like case with MPO approximation, and the right panel is a log-log plot of $\eta_n(D)$ of the LDOS-case with MPS approximation. The system size is $N = 40$ for the upper figures and $N = 80$ for the lower.

operator

$$\eta_n(D) = \frac{\left|\left||t_n^{(D_0)}\rangle\left(\tilde{H}\right) - |t_n^{(D)}\rangle\left(\tilde{H}\right)\right|\right|_2^2}{\left|\left||t_n^{(D_0)}\rangle\left(\tilde{H}\right)\right|\right|_2^2}. \tag{4.50}$$

With these we are able to estimate the bond dimension $D$ required to keep the truncation error below a certain threshold at expansion order $n$. This $n$ *vs.* $D$ dependence for the non-integrable Ising chain is shown in Fig. 4.7. It is surprising to find that the bond dimension needed for $N = 80$ seems to be smaller than that for $N = 40$, which supports the efficiency of our method in the thermodynamic limit.

The results suggest an exponential scaling for the DOS-like case (semi-log plot in the left) and a polynomial scaling for the LDOS-like case (log-log plot in the right). It is in general more costly to compute the full DOS than to retrieve the single state LDOS. This scaling can be viewed from another perspective, the time evolution application after a Fourier (for real

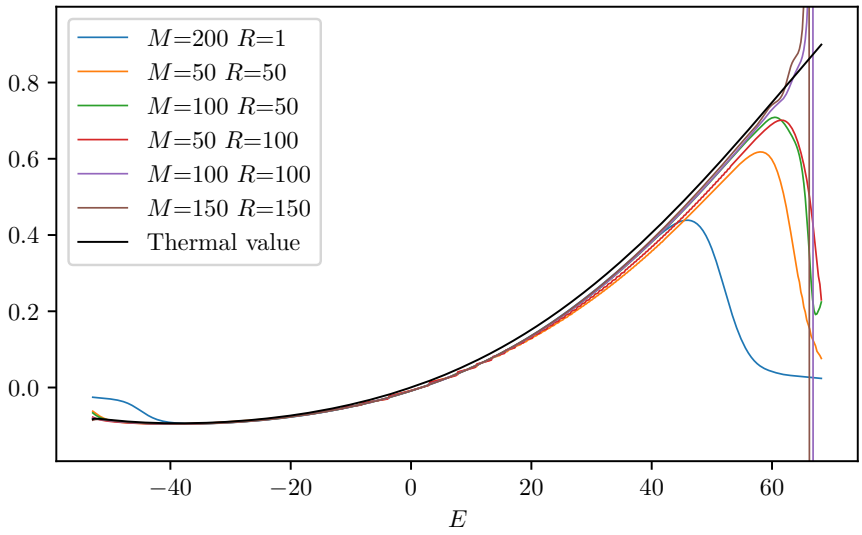


Figure 4.8: Full spectrum version of the upper left plot in Fig. 4.5 ($(\sigma^z_{N/2})_{M,R}(E)$ of the non-integrable Ising model), with more choices of $M$ and $R$.

time evolution) or Laplace (for imaginary time evolution) transform. The error of $\mathrm{tr}(\hat{O}e^{-iHt}) = \int e^{-iEt}g(E,\hat{O})\mathrm{d}t$ will be of order $\mathcal{O}(t/M)$ given that the bond dimension truncation error is small. Therefore to reach time $t$, it is required that $M = \mathcal{O}(t)$ (also see Appendix 6.2). Therefore the the scaling of upper bond of required bond dimension, $D = \mathcal{O}(e^t)$, is exactly the same as in the TEBD algorithm, where the scaling of the required $D$ comes from the linear growth of the entanglement entropy with time during the evolution. Our results suggest that, in the LDOS-like case, it could even be lowered to $D = \mathcal{O}(\mathrm{poly}(t))$.

When computing $O_{M,R}(E)$, the error additionally comes from another Chebyshev cutoff of step function at order $R$. At the far edges of the spectrum, even after applying the step function strategy, $O_{M,R}$ still diverges or oscillates quickly. It might be due to the sparsity of states in the tails, and we cut 2%-3% of the spectrum on both sides in Fig. 4.5 and Fig. 4.6 that probe thermal properties. In Fig. 4.8, a full spectrum version is shown.

# Chapter 5

# Conclusion and Outlook

In this report we presented a technique based on Chebyshev expansions and tensor network algorithms to compute generalized densities of states, which encode dynamical properties, for one-dimensional quantum many body models. We have also shown that this technique allows

- probing directly the thermalization of given initial states and
- probing weak ETH through comparing the canonical and microcanonical values of given local observables.

It avoids the difficulty in explicitly simulating long time evolution, and can reach much larger system sizes than any direct simulations having been achieved so far. Applications to the integrable and non-integrable Ising models and the PXP model are illustrated as examples, and the results fit well with expectations from theory and exact diagonalization in small systems.

It is a general method and a broad range of potential extensions and applications can be analyzed in the future:

- First of all, our calculations apply to all systems whose Hamiltonians can be written as MPO, and even PEPO in two-dimensional systems. For instance, it could be possible to find appropriate observables to detect and explore more features of many body localization, when it comes to disordered or quasi-periodic systems.
- Secondly, beyond various Hamiltonians our scheme also carries over to any sort of observable as an MPO in GDOS. It could be useful to explore the spectral properties of Lindbladians, random MPO, *etc.*

- Finally, the scheme used to compute the survival probability can also be extended to monitor the evolution of observables, even for initial mixed states at finite temperatures (Appendix 6.2). It thus provides new tools to study the fundamental questions of out-of-equilibrium dynamics.

The Chebyshev expansion can also be substituted by other approximations for the $\delta$ operators. One choice is the cosine filter (Ge et al., 2019) which expands it as a time series, *i.e.*, a sum of time evolution operators. An algorithm based on the cosine filter has been designed for quantum simulators (Lu et al., 2020). It can also be implemented on classical computers with no worries of the sign problem, which samples over states in a computational basis to approximate the trace in $\mathrm{tr}\left(\delta(E-\hat{H})\hat{O}\right)$. The algorithm allows more freedom in the choice of observables, as they are no longer required to be MPO; the problem of exponentially small DOS near the edges of spectrum could also be avoided. The cost is that we have to however probe once for each energy $E$.

# Chapter 6

# Appendix

## 6.1 Proofs of the thermodynamic limits of GDOS

In this section, we present proofs of theorem 2.2 and theorem 2.3 in section 2.2.1, which give the thermodynamic limits of GDOS.

### 6.1.1 Proof of theorem 2.2

Consider a local, bounded Hamiltonian of a spin chain with energy eigenstate decomposition

$$\hat{H}_N = \sum_{i=1}^{N} \hat{\mathcal{H}}_i = \sum_n E_n \left|n\right\rangle \left\langle n\right|, \tag{6.1}$$

where

$$\hat{\mathcal{H}}_i = \mathbb{1}^{\otimes i-1} \otimes \hat{h}_i \otimes \mathbb{1}^{\otimes N-i} + \mathbb{1}^{\otimes i-1} \otimes \hat{g}_{i,i+1} \otimes \mathbb{1}^{\otimes N-i-1} \tag{6.2}$$

and $||\mathcal{H}_i|| \leq C$ for all $1 \leq i \leq N$. We assume open boundary conditions $\hat{g}_{N,N+1} = 0$.

**Theorem.** *(Gaussian LDOS (Hartmann et al., 2004).) Let $\left|a\right\rangle = \otimes_{i=1}^{N} \left|a_i\right\rangle$ be a product state with mean energy $E_a = \langle a|\hat{H}|a\rangle$ and variance $\sigma_a^2 = \langle a|\hat{H}^2|a\rangle - E_a^2$. If $\sigma_a^2 \geq \Delta \cdot N$ for some constant $\Delta > 0$, then the measure defined by LDOS*

$$P_a\left(E \in [E_1, E_2]\right) = \int_{E_1}^{E_2} g(E,a)\mathrm{d}E = \sum_{|n\rangle : E_1 \leq E_n \leq E_2} \left|\left\langle a|n\right\rangle\right|^2 \tag{6.3}$$

*converges weakly to normal distribution in the thermodynamic limit:*

$$\lim_{N\to\infty} P_a\left(E\in[E_1,E_2]\right)=\frac{1}{\sqrt{2\pi}\sigma_a}\int_{E_1}^{E_2}\exp\left[-\frac{(E-E_a)^2}{2\sigma_a^2}\right]\mathrm{d}E \tag{6.4}$$

*for any* $-\infty<E_1<E_2<\infty$.

*Proof.* For convenience, we shift and rescale the Hamiltonian by defining

$$\hat{X}_N=\frac{\hat{H}_N-\langle a|\hat{H}_N|a\rangle}{\sigma_a}=\sum_{i=1}^{N}\hat{\mathcal{X}}_i,\quad \hat{\mathcal{X}}_i=\frac{\hat{\mathcal{H}}_i-\langle a|\hat{\mathcal{H}}_i|a\rangle}{\sigma_a}. \tag{6.5}$$

Therefore $||\mathcal{X}_i||\leq 2C/\sigma_a$. As the system is nearest neighbor interacting, it is sufficient to take single sites as links. The length of blocks $k-1$ should be chosen

- small enough so that we can apply central limit theorem to $[N/k]$ blocks ($[x]:=\max\{n\in\mathbb{Z}|n\leq x\}$), and hence $\lim_{N\to\infty}k/N=0$;
- large enough so that the links become minor significant, which we will see later means $\lim_{N\to\infty}N/k^2=0$.

A possible choice is $k=[N^{3/4}]$. The blocks are given by

$$\hat{\mathcal{B}}_j=\sum_{i=1}^{q}\hat{\mathcal{X}}_{(j-1)\cdot k+i},\quad q=\begin{cases}k-1, & j=1,\cdots,[N/k];\\ N-k\cdot[N/k], & j=[N/k]+1.\end{cases} \tag{6.6}$$

The (rescaled) Hamiltonian is thus separated into the blocks and links:

$$\hat{X}_N=\hat{B}_N+\hat{L}_N,\quad \hat{B}_N=\sum_{j=1}^{[N/k]+1}\hat{\mathcal{B}}_j,\quad \hat{L}_N=\sum_{j=1}^{[N/k]}\hat{\mathcal{X}}_{j\cdot k}. \tag{6.7}$$

We want to show that the links can be neglected in the thermodynamic limit when computing the characteristic function $\langle a|e^{-it\hat{X}_N}|a\rangle$. The characteristic function encodes the full statistical information of $|a\rangle$ with regard to the Hamiltonian and, in particular, its Fourier transform is the LDOS. Use the operator identity

$$e^{-it(\hat{A}+\hat{B})}=e^{-it\hat{A}}-i\int_0^t e^{-i(t-s)(\hat{A}+\hat{B})}\hat{B}e^{-is\hat{A}}\mathrm{d}s, \tag{6.8}$$

the difference can be bounded pointwise by

$$\begin{aligned}\left|\langle a|e^{-it\hat{X}_N}-e^{-it\hat{B}_N}|a\rangle\right| &\le \left|\int_0^t \langle a|e^{-i(t-s)\hat{X}_N}\hat{L}_N e^{-is\hat{B}_N}|a\rangle\,\mathrm{d}s\right| \\ &\le \int_0^t \left|\langle a|e^{-i(r-s)\hat{X}_N}\hat{L}_N e^{-is\hat{B}_N}|a\rangle\right|\mathrm{d}s \\ &\le \int_0^t \sqrt{\langle a|e^{is\hat{B}_N}\hat{L}_N^2 e^{-is\hat{B}_N}|a\rangle}\mathrm{d}s \\ &\le \int_0^t \sqrt{\left|\left|\hat{L}_N^2\right|\right|}\mathrm{d}s \le t\sqrt{\left[\frac{N}{k}\right]^2\cdot\left(\frac{2C}{\sigma_a}\right)^2} \\ &\le t\sqrt{\frac{N}{k^2}\cdot\frac{(2C)^2}{\Delta}} \xrightarrow{N\to\infty} 0.\end{aligned} \tag{6.9}$$

In the third step, the Cauchy Schwartz inequality $|\langle\psi|\phi\rangle| \le \sqrt{\langle\psi|\psi\rangle\langle\phi|\phi\rangle}$ is used, where $|\psi\rangle = e^{i(t-s)\hat{X}_N}|a\rangle$ and $|\phi\rangle = \hat{L}_N e^{-is\hat{B}_N}|a\rangle$.

It is now sufficient to deal with $\hat{B}_N$, which will give the same LDOS of $|a\rangle$ as that with $\hat{X}_N$ in the thermodynamic limit. Since $\hat{B}_N$ factorizes, the (classical) Lyapunov central limit theorem (Billingsley, 1999) is applicable. For a sequence of independent random variables $x_1, \cdots, x_n$, each with finite mean value $\mu_i$ and variance $\sigma_i^2$, define $s_n^2 = \sum_{i=1}^n \sigma_i^2$. If for some $\delta > 0$, the Lyapunov condition

$$\lim_{n\to\infty}\frac{1}{s_n^{2+\delta}}\sum_{i=1}^n E\left[|x_i-\mu_i|^{2+\delta}\right] = 0 \tag{6.10}$$

is satisfied, then the sum of the random variables converges weakly to normal distribution:

$$\frac{1}{s_n}\sum_{i=1}^n (x_i-\mu_i) \xrightarrow{d} N(0,1). \tag{6.11}$$

Here $\hat{\mathcal{B}}_i$ are the random variables that can take its eigenvalue $b_{i,l}$ at probability $|\langle a|e_{i,l}\rangle|^2$, where $|e_{i,l}\rangle$ is the corresponding eigenstate. Hence $n = [N/k]+1$, $\mu_i = \langle a|\hat{\mathcal{B}}_i|a\rangle = 0$ and

$$s_n^2 = \sum_{i=1}^n \langle a|\hat{\mathcal{B}}_i^2|a\rangle = \langle a|\hat{B}_N^2|a\rangle = -\frac{\partial^2}{\partial t^2}\langle a|e^{-it\hat{B}_N}|a\rangle\,. \tag{6.12}$$

According to Eq. (6.9), $\lim_{N\to\infty} s_n^2 = \langle a|\hat{X}_N^2|a\rangle = 1$. The rest is to compute $\langle a|\hat{\mathcal{B}}_i^{2+\delta}|a\rangle$, where we choose $\delta = 2$:

$$\begin{aligned}\langle a|\hat{\mathcal{B}}_i^4|a\rangle &= \sum_{\mu,\nu,\rho,\tau=1}^{k-1} \langle a|\hat{\mathcal{X}}_{(i-1)\cdot k+\mu}\hat{\mathcal{X}}_{(i-1)\cdot k+\nu}\hat{\mathcal{X}}_{(i-1)\cdot k+\rho}\hat{\mathcal{X}}_{(i-1)\cdot k+\tau}|a\rangle \\ &\leq \left(\frac{2C}{\sigma_a}\right)^4 \cdot 3 \cdot [3k-5]^2 \leq \frac{3^3\cdot 16C^4}{\Delta^2}\cdot\left(\frac{k}{N}\right)^2.\end{aligned} \tag{6.13}$$

The estimation comes from the fact that the sites in non-vanishing terms can form two identical or neighboring pairs. There are 3 choices of pairs and for each pair, $3k-5$ possibilities (we over count here). Thus

$$\frac{1}{s_n^4}\sum_{i=1}^{n}\langle a|\hat{\mathcal{B}}_i^4|a\rangle \leq \frac{3^3\cdot 16C^4}{\Delta^2}\cdot\left(\left[\frac{N}{k}\right]+1\right)\cdot\left(\frac{k}{N}\right)^2 \xrightarrow{n\to\infty} 0. \tag{6.14}$$

Finally we draw the conclusion

$$\lim_{N\to\infty}\int_{E_1}^{E_2} g(E,a)\mathrm{d}E = \frac{1}{\sqrt{2\pi}\sigma_a}\int_{E_1}^{E_2}\exp\left[-\frac{(E-E_a)^2}{2\sigma_a^2}\right]\mathrm{d}E. \tag{6.15}$$

□

### 6.1.2 Proof of theorem 2.3

Consider a general spin-1/2 chain

$$\hat{\mathcal{H}}_i = \sum_{a=0}^{3}\sum_{b=1}^{3}\alpha_{a,b,i}\hat{\sigma}_i^{(a)}\hat{\sigma}_{i+1}^{(b)}, \tag{6.16}$$

where $\hat{\sigma}^{(a)}$ $(a=0,1,2,3)$ form the orthonormal Pauli basis of the local Hilbert space. Assume the normalization condition

$$\frac{1}{2^N}\mathrm{tr}\left(\hat{H}_N^2\right) = \sum_{i=1}^{N}\sum_{a=0}^{3}\sum_{b=1}^{3}\alpha_{a,b,i}^2 =: N\alpha^2. \tag{6.17}$$

Let $\hat{O}$ be a local spin-1/2 hermitian operator for $s$ neighboring sites with eigenspace decomposition

$$\hat{O} = \sum_{m=1}^{2^s}\tilde{O}_m\hat{P}_m. \tag{6.18}$$

$\tilde{O}_m \in \mathbb{R}$ are its eigenvalues and $\hat{P}_m$ are projectors onto corresponding eigenspaces. We want to measure $\hat{O}$ on a spin-1/2 chain of length $N$ from the $q_N$-th site, with $\hat{O}_N = \mathbb{1}^{\otimes q_N} \otimes \hat{O} \otimes \mathbb{1}^{\otimes N-q_N-s}$ and $\hat{P}_{N,m} = \mathbb{1}^{\otimes q_N} \otimes \hat{P}_m \otimes \mathbb{1}^{\otimes N-q_N-s}$.

**Theorem.** *(GDOS as a sum of Gaussians.) If the limit*

$$\lim_{N\to\infty} \operatorname{tr}\left(\sum_{j=q_N-1}^{q_N+s} \mathcal{H}_j \hat{P}_{N,m}\right) = E_m \tag{6.19}$$

*exists for all $m$, then*

$$\lim_{N\to\infty} \int_{E_1}^{E_2} g(E, \hat{O}_N)\mathrm{d}E = \frac{2^{N-s}}{\sqrt{2\pi N}\alpha} \sum_m \tilde{O}_m \int_{E_1}^{E_2} e^{-(E-E_m)^2/2N\alpha^2}\mathrm{d}E \tag{6.20}$$

*for any $-\infty < E_1 < E_2 < \infty$.*

*Proof.* We again want to divide the chain into blocks and links between them to make use of the Lyapunov central limit theorem. The main difference from the LDOS case is to take traces with regard to projectors $\hat{P}_{N,m}$ instead of measuring with a product state $|a\rangle$:

$$\operatorname{tr}\left(\delta(E-\hat{H}_N)\,|a\rangle\,\langle a|\right) \to \sum_m \tilde{O}_m \operatorname{tr}\left(\delta(E-\hat{H}_N)\hat{P}_{N,m}\right). \tag{6.21}$$

Since $\operatorname{tr}\left(\hat{P}_{N,m}\right) = 2^{N-s}$, the probability measure obtained from GDOS is

$$P_{\hat{P}_{N,m}}(E \in [E_1, E_2]) = \frac{1}{2^{N-1}} \int_{E_1}^{E_2} g(E, \hat{P}_{N,m})\mathrm{d}E. \tag{6.22}$$

For convenience, the Hamiltonian is again rescaled by $\alpha\sqrt{N}$ to

$$\hat{X}_N = \sum_{i=1}^{N} \hat{\mathcal{X}}_i. \tag{6.23}$$

The block and link parts of Hamiltonians are also defined as in the proof of Theorem 2.2. The conditions of length $k$ of a block can however be loosened

to $\lim_{N\to\infty} k/N = 0$ and $\lim_{N\to\infty} 1/k = 0$, as can be seen from the difference of characteristic functions:

$$\begin{aligned}
&\left|\frac{1}{2^{N-s}}\mathrm{tr}\left(e^{it\hat{X}_N}\hat{P}_{N,m}\right) - \frac{1}{2^{N-s}}\mathrm{tr}\left(e^{it\hat{B}_N}\hat{P}_{N,m}\right)\right| \\
\leq&\frac{1}{2^{N-s}}\int_0^t \left|\mathrm{tr}\left(e^{-i(t-s)\hat{X}_N}\hat{L}_N e^{-is\hat{B}_N}\hat{P}_{N,m}\right)\right| \mathrm{d}s \\
\leq&\frac{1}{2^{N-s}}\int_0^t \sqrt{\mathrm{tr}\left(\hat{L}_N^2\right)\mathrm{tr}\left(\hat{P}_{N,m}^2\right)}\mathrm{d}s = t\sqrt{\frac{1}{2^{N-s}}\mathrm{tr}\left(\hat{L}_N^2\right)} \\
\leq&t\sqrt{\frac{1}{2^{N-s}}\sum_{j=1}^{[N/k]}\sum_{a=0}^{3}\sum_{b=1}^{3}\frac{\alpha_{a,b,j\cdot k}^2}{\alpha^2 N}\cdot 2^N} \\
\leq&t\sqrt{2^s\left[\frac{N}{k}\right]\frac{12(C')^2}{\alpha^2 N}} \xrightarrow{N\to\infty} 0.
\end{aligned} \tag{6.24}$$

Since $k \to \infty$ as $N \to \infty$, we can always shift the position of blocks and links such that the sites $q_N + 1, \cdots, q_N + s$ lie in the same block labeled by $j_o = [q_N + 1/k] + 1$. The corresponding first order moment $\frac{1}{2^{N-s}}\mathrm{tr}\left(\hat{\mathcal{B}}_{j_o}\hat{P}_{N,m}\right)$ becomes nonzero, which will shift the centre of the Gaussian. Using the same trick, the total variance $s_n^2$ can be calculated from the full Hamiltonian:

$$\begin{aligned}
|s_n^2 - 1| =& \left|\frac{1}{2^{N-s}}\mathrm{tr}\left(\hat{X}_N^2\hat{P}_{N,m}\right) - \frac{1}{2^N}\mathrm{tr}\left(\hat{X}_N^2\right)\right| \\
=& \left|\mathrm{tr}\left[\left(\hat{\mathcal{X}}_{j_o}^2 + \left\{\hat{\mathcal{X}}_{j_o-1}, \hat{\mathcal{X}}_{j_o}\right\} + \left\{\hat{\mathcal{X}}_{j_o+1}, \hat{\mathcal{X}}_{j_o}\right\}\right)\left(\frac{\hat{P}_{N,m}}{2^{N-s}} - \frac{\mathbb{1}}{2^N}\right)\right]\right| \\
\leq& \frac{10\cdot(12C')^2}{\alpha^2 N} \xrightarrow{N\to\infty} 0.
\end{aligned} \tag{6.25}$$

The computation of the fourth order $\frac{1}{2^{N-s}}\mathrm{tr}\left(\hat{\mathcal{B}}_j^4\hat{P}_{N,m}\right)$ is similar, which has a correction of order $\mathcal{O}(1/N^2)$ from $\frac{1}{2^N}\mathrm{tr}\left(\hat{\mathcal{B}}_j^4\right)$, where

$$\left|\frac{1}{2^N}\mathrm{tr}\left(\hat{\mathcal{B}}_j^4\right)\right| \leq 3^3 k^2\left(\frac{12C'}{\alpha\sqrt{N}}\right)^4. \tag{6.26}$$

Therefore $\sum_{j=1}^{N}\frac{1}{2^{N-s}}\mathrm{tr}\left(\hat{\mathcal{B}}_j^4\hat{P}_{N,m}\right) = \mathcal{O}(k/N)$ and the Lyapunov condition is still satisfied. □

## 6.2 Time evolution with KPM

In this section, we discuss simulating time evolutions with KPM. We have shown how to compute the Loschmidt echos by doing Fourier transforms to the LDOS. The time evolved observables can also be related to the spectral properties by means of Fourier transforms. The expectation value of an observable $\hat{O}$ in a time evolved state $\hat{\rho}(t) = e^{-i\hat{H}t}\hat{\rho}e^{i\hat{H}t}$ can be written as

$$\begin{aligned} O(t) &= \mathrm{tr}\left(e^{-i\hat{H}t}\hat{\rho}e^{i\hat{H}t}\hat{O}\right) = \sum_{k,k'} e^{-i(E_k - E_{k'})t} \langle k'|\hat{O}|k\rangle \langle k|\hat{\rho}|k'\rangle \\ &= \int e^{-iEt} \sum_{k,k'} \delta(E - E_k + E_{k'}) \langle k'|\hat{O}|k\rangle \langle k|\hat{\rho}|k'\rangle \,\mathrm{d}E \\ &= \int e^{-iEt} \langle \hat{O}|\delta(E - \hat{H}\otimes\mathbb{1} + \mathbb{1}\otimes\hat{H}^*)|\hat{\rho}\rangle \,\mathrm{d}E, \end{aligned} \tag{6.27}$$

where $\langle\hat{O}|$ and $|\hat{\rho}\rangle$ viewed as vectors with double physical indices, as we did for transforming MPO into MPS. Note that $\hat{\rho}$ could either be a pure state or a mixed state at finite temperatures. The LDOS-like Chebyshev expansion with effective Hamiltonian $\hat{H}_{\mathrm{eff}} = \hat{H}\otimes\mathbb{1} - \mathbb{1}\otimes\hat{H}^*$ can be done, which leads to the same form of $O(t)$ as in Eq. (4.42):

$$O(t) \approx O_M(t) = \frac{1}{\nu}\left[\gamma_0\mu_0 J_0(-\nu t) + 2\sum_{n=1}^{M-1} i^n \gamma_n \mu_n J_n(-\nu t)\right], \tag{6.28}$$

where $\mu_n = \langle\hat{O}|T_n(\tilde{H}_{\mathrm{eff}})|\hat{\rho}\rangle$.

Unlike the GDOS, $O(t)$ without any approximation are usually already smooth functions and thus the kernels might not improve the results as well after a Fourier transform. In Fig. 6.1, an example using different kernels is presented. The curve with trivial Dirichlet kernel, regardless of the oscillations after deviation, fits the exact values for the longest time with the same order of expansion.

The error of such bare Bessel function series can be bounded by the

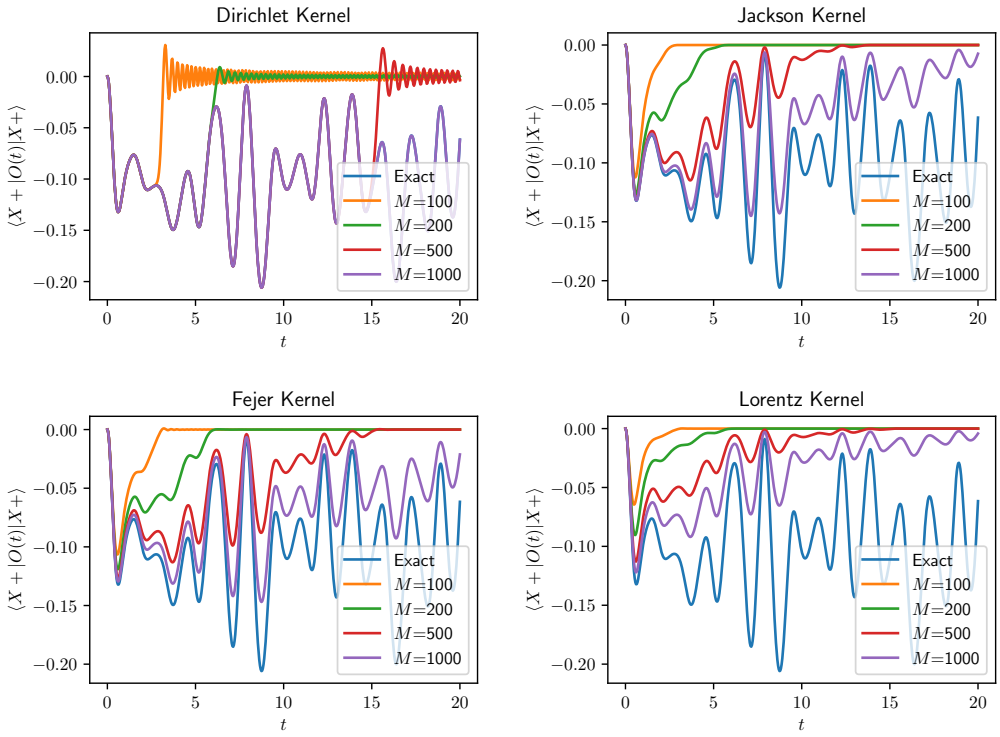


Figure 6.1: Chebyshev time evolution with different kernels. It is the Ising model with $(J, g, h) = (1, -1.05, 0.5)$ and system size $N = 10$. The initial state is $\hat{\rho} = |X+\rangle \langle X+|$ and $\hat{O} = \hat{\sigma}^z_{N/2}$. For Lorentz kernel, $\lambda = 4$. All results are calculated with exact diagonalization.

remainder of Taylor expansion (Koskela and Jarlebring, 2017):

$$\begin{aligned}\epsilon = &\left|\frac{1}{\nu}2\sum_{n=M}^{\infty} i^n \mu_n J_n(-\nu t)\right| \leq \frac{||\mu||}{\nu}\sum_{n=M}^{\infty}\frac{(2\nu t)^n}{n!}\\ \leq &\frac{||\mu||}{\nu}\frac{(2\nu t)^M}{M!}e^{2\nu t}\\ \approx &\frac{||\mu||}{\nu\sqrt{2\pi M}}\left(\frac{2\nu t e}{M}\right)^M e^{2\nu t}.\end{aligned} \tag{6.29}$$

$||\mu||$ refers to $\sup \mu_n$. To obtain a fixed error $\epsilon$, $M = \mathcal{O}(t)$ is required. Actually when $M > 2\alpha\nu e t$, where $\alpha \ln \alpha = 1/e$, $\epsilon \lesssim ||\mu|| / \nu\sqrt{2\pi M} = \mathcal{O}(1/\sqrt{t})$. The linear dependence can be checked in the upper left plot in Fig. 6.1, where $t_{\max,M} \approx 3M/100$.

# Bibliography


Dmitry A. Abanin, Ehud Altman, Immanuel Bloch, and Maksym Serbyn. Many-body localization, thermalization, and entanglement. *Reviews of Modern Physics*, 91(2):21001, 2018.

Luigi Accardi. Topics in quantum probability. *Physics Reports*, 77(3):169–192, 1981.

Ian Affleck, Tom Kennedy, Elliott H. Lieb, and Hal Tasaki. Rigorous results on valence-bond ground states in antiferromagnets. *Physical Review Letters*, 59(7):799–802, 1987.

P. W. Anderson. Absence of Diffusion in Certain Random Lattices. *Physical Review*, 109(5):1492–1505, 1958.

Mari Carmen Bañuls, J. I. Cirac, and M. B. Hastings. Strong and Weak Thermalization of Infinite Nonintegrable Quantum Systems. *Physical Review Letters*, 106(5):050405, 2011.

M.C. Bañuls, K. Cichy, J.I. Cirac, and K. Jansen. The mass spectrum of the Schwinger model with matrix product states. *Journal of High Energy Physics*, 2013(11):158, 2013.

Jens H. Bardarson, Frank Pollmann, and Joel E. Moore. Unbounded Growth of Entanglement in Models of Many-Body Localization. *Physical Review Letters*, 109(1):017202, 2012.

Charles H Bennett, Herbert J Bernstein, Sandu Popescu, and Benjamin Schumacher. Concentrating partial entanglement by local operations. *Physical Review A*, 53(4):2046–2052, 1996.

Hannes Bernien, Sylvain Schwartz, Alexander Keesling, Harry Levine, Ahmed Omran, Hannes Pichler, Soonwon Choi, Alexander S. Zibrov, Manuel Endres, Markus Greiner, Vladan Vuletić, and Mikhail D. Lukin. Probing many-body dynamics on a 51-atom quantum simulator. *Nature*, 551(7682):579–584, 2017.

Patrick Billingsley. *Convergence of Probability Measures*. Wiley Series in Probability and Statistics. John Wiley & Sons, Inc., Hoboken, NJ, USA, 1999.

Pasquale Calabrese and John Cardy. Evolution of entanglement entropy in one-dimensional systems. *Journal of Statistical Mechanics: Theory and Experiment*, 2005(04):P04010, 2005.

C. Canuto and A. Quarteroni. Approximation Results for Orthogonal Polynomials in Sobolev Spaces. *Mathematics of Computation*, 38(157):67, 1982.

J.-y. Choi, S. Hild, J. Zeiher, P. Schauss, A. Rubio-Abadal, T. Yefsah, V. Khemani, D. A. Huse, I. Bloch, and C. Gross. Exploring the many-body localization transition in two dimensions. *Science*, 352(6293):1547–1552, 2016.

Ignacio Cirac, David Perez-Garcia, Norbert Schuch, and Frank Verstraete. Matrix Product States and Projected Entangled Pair States: Concepts, Symmetries, and Theorems. pages 1–71, 2020.

J. Ignacio Cirac, D. Pérez-García, N Schuch, and F Verstraete. Matrix product density operators: Renormalization fixed points and boundary theories. *Annals of Physics*, 378:100–149, 2017.

Luca D'Alessio, Yariv Kafri, Anatoli Polkovnikov, and Marcos Rigol. From quantum chaos and eigenstate thermalization to statistical mechanics and thermodynamics. *Advances in Physics*, 65(3):239–362, 2016.

J. M. Deutsch. Quantum statistical mechanics in a closed system. *Physical Review A*, 43(4):2046–2049, 1991.

Joshua M. Deutsch. Eigenstate thermalization hypothesis. *Reports on Progress in Physics*, 81(8):082001, 2018.

J Dukelsky, M. A Martín-Delgado, T Nishino, and G Sierra. Equivalence of the variational matrix product method and the density matrix renormalization group applied to spin chains. *Europhysics Letters (EPL)*, 43(4): 457–462, 1998.

J Eisert, M. Cramer, and M. B. Plenio. Colloquium : Area laws for the entanglement entropy. *Reviews of Modern Physics*, 82(1):277–306, 2010.

Tilman Enss and Jesko Sirker. Light cone renormalization and quantum quenches in one-dimensional Hubbard models. *New Journal of Physics*, 14 (2):023008, 2012.

M. Falcioni, U. Marini Bettolo Marconi, and A. Vulpiani. Ergodic properties of high-dimensional symplectic maps. *Physical Review A*, 44(4):2263–2270, 1991.

Leopold Fejér. Untersuchungen über Fouriersche Reihen. *Mathematische Annalen*, 58(1-2):51–69, 1903.

Johannes Feldmeier, Frank Pollmann, and Michael Knap. Emergent Glassy Dynamics in a Quantum Dimer Model. *Physical Review Letters*, 123(4): 040601, 2019.

W. M. C. Foulkes, L. Mitas, R. J. Needs, and G. Rajagopal. Quantum Monte Carlo simulations of solids. *Reviews of Modern Physics*, 73(1):33–83, 2001.

Yimin Ge, Jordi Tura, and J. Ignacio Cirac. Faster ground state preparation and high-precision ground energy estimation with fewer qubits. *Journal of Mathematical Physics*, 60(2):022202, 2019.

Christian Gogolin. *Equilibration and thermalization in quantum systems*. PhD thesis, Freie Universität Berlin, 2014.

Emanuel Gull, Andrew J. Millis, Alexander I. Lichtenstein, Alexey N. Rubtsov, Matthias Troyer, and Philipp Werner. Continuous-time Monte Carlo methods for quantum impurity models. *Reviews of Modern Physics*, 83(2):349–404, 2011.

Jad C. Halimeh, Fabian Kolley, and Ian P. McCulloch. Chebyshev matrix product state approach for time evolution. *Physical Review B*, 92(11): 115130, 2015.

Michael Hartmann, Günter Mahler, and Ortwin Hess. Gaussian Quantum Fluctuations in Interacting Many Particle Systems. *Letters in Mathematical Physics*, 68(2):103–112, 2004.

Michael Hartmann, Günter Mahler, and Ortwin Hess. Spectral densities and partition functions of modular quantum systems as derived from a central limit theorem. *Journal of Statistical Physics*, 119(5-6):1139–1151, 2005.

Michael J. Hartmann, Javier Prior, Stephen R. Clark, and Martin B. Plenio. Density Matrix Renormalization Group in the Heisenberg Picture. *Physical Review Letters*, 102(5):057202, 2009.

M B Hastings. An area law for one-dimensional quantum systems. *Journal of Statistical Mechanics: Theory and Experiment*, 2007(08):P08024–P08024, 2007.

M. B. Hastings and R. Mahajan. Connecting entanglement in time and space: Improving the folding algorithm. *Physical Review A*, 91(3):032306, 2015.

Naomichi Hatano and Masuo Suzuki. Finding Exponential Product Formulas of Higher Orders. volume 68, pages 37–68. 2005.

Wen Wei Ho, Soonwon Choi, Hannes Pichler, and Mikhail D. Lukin. Periodic Orbits, Entanglement, and Quantum Many-Body Scars in Constrained Models: Matrix Product State Approach. *Physical Review Letters*, 122(4): 40603, 2019.

Andreas Holzner, Andreas Weichselbaum, Ian P. McCulloch, Ulrich Schollwöck, and Jan von Delft. Chebyshev matrix product state approach for spectral functions. *Physical Review B*, 83(19):195115, 2011.

David A. Huse, Rahul Nandkishore, Vadim Oganesyan, Arijeet Pal, and S. L. Sondhi. Localization-protected quantum order. *Physical Review B*, 88(1): 014206, 2013.

Dunham Jackson. *Über die Genauigkeit der Annäherung stetiger Funktionen durch ganze rationale Funktionen gegebenen Grades und trigonometrische Summen gegebener Ordnung*. PhD thesis, Göttingen University, 1911.

Andrew J.A. James, Robert M. Konik, and Neil J. Robinson. Nonthermal States Arising from Confinement in One and Two Dimensions. *Physical Review Letters*, 122(13):130603, 2019.

A. M. Kaufman, M. E. Tai, A. Lukin, M. Rispoli, R. Schittko, P. M. Preiss, and M. Greiner. Quantum thermalization through entanglement in an isolated many-body system. *Science*, 353(6301):794–800, 2016.

J. P. Keating, N. Linden, and H. J. Wells. Spectra and Eigenstates of Spin Chain Hamiltonians. *Communications in Mathematical Physics*, 338(1): 81–102, 2015.

Vedika Khemani, Chris R. Laumann, and Anushya Chandran. Signatures of integrability in the dynamics of Rydberg-blockaded chains. *Physical Review B*, 99(16):161101, 2019.

Hyungwon Kim, Mari Carmen Bañuls, J. Ignacio Cirac, Matthew B. Hastings, and David A. Huse. Slowest local operators in quantum spin chains. *Physical Review E*, 92(1):012128, 2015.

Marton Kormos, Mario Collura, Gabor Takács, and Pasquale Calabrese. Real-time confinement following a quantum quench to a non-integrable model. *Nature Physics*, 13(3):246–249, 2017.

Antti Koskela and Elias Jarlebring. On a generalization of the Bessel function Neumann expansion. pages 1–8, 2017.

Tomotaka Kuwahara, Álvaro M. Alhambra, and Anurag Anshu. Improved Thermal Area Law and Quasilinear Time Algorithm for Quantum Gibbs States. *Physical Review X*, 11(1):011047, 2021.

Zhihao Lan, Merlijn van Horssen, Stephen Powell, and Juan P. Garrahan. Quantum Slow Relaxation and Metastability due to Dynamical Constraints. *Physical Review Letters*, 121(4):040603, 2018.

Elliott H Lieb and Derek W Robinson. The finite group velocity of quantum spin systems. *Communications in Mathematical Physics*, 28(3):251–257, 1972.

Cheng-ju Lin. *Surviving Quantum Chaos : Weak Thermalization , Prethermalization and Quantum Many-Body Scar States Thesis by*. Ph.d.thesis, 2019.

Cheng-Ju Lin and Olexei I. Motrunich. Quasiparticle explanation of the weak-thermalization regime under quench in a nonintegrable quantum spin chain. *Physical Review A*, 95(2):023621, 2017.

Sirui Lu, Mari Carmen Bañuls, and J. Ignacio Cirac. Algorithms for quantum simulation at finite energies. pages 1–18, 2020.

David J. Luitz, Nicolas Laflorencie, and Fabien Alet. Many-body localization edge in the random-field Heisenberg chain. *Physical Review B*, 91(8): 081103, 2015.

Ian P McCulloch. From density-matrix renormalization group to matrix product states. *Journal of Statistical Mechanics: Theory and Experiment*, 2007(10):P10014–P10014, 2007.

Andras Molnar, Norbert Schuch, Frank Verstraete, and J. Ignacio Cirac. Approximating Gibbs states of local Hamiltonians efficiently with projected entangled pair states. *Physical Review B*, 91(4):045138, 2015.

Stellan Östlund and Stefan Rommer. Thermodynamic Limit of Density Matrix Renormalization. *Physical Review Letters*, 75(19):3537–3540, 1995.

Arijeet Pal and David A. Huse. Many-body localization phase transition. *Physical Review B*, 82(17):174411, 2010.

Nicola Pancotti, Giacomo Giudice, J. Ignacio Cirac, Juan P. Garrahan, and Mari Carmen Bañuls. Quantum East Model: Localization, Nonthermal Eigenstates, and Slow Dynamics. *Physical Review X*, 10(2):021051, 2020.

B Pirvu, V Murg, J I Cirac, and F Verstraete. Matrix product operator representations. *New Journal of Physics*, 12(2):025012, 2010.

Sandu Popescu, Anthony J. Short, and Andreas Winter. Entanglement and the foundations of statistical mechanics. *Nature Physics*, 2(11):754–758, 2006.

Marcos Rigol, Vanja Dunjko, and Maxim Olshanii. Thermalization and its mechanism for generic isolated quantum systems. *Nature*, 452(7189):854–858, 2008.

Mauro Schiulaz, E. Jonathan Torres-Herrera, and Lea F. Santos. Thouless and relaxation time scales in many-body quantum systems. *Physical Review B*, 99(17):174313, 2019.

Ulrich Schollwöck. The density-matrix renormalization group in the age of matrix product states. *Annals of Physics*, 326(1):96–192, 2011.

Michael Schreiber, Sean S. Hodgman, Pranjal Bordia, H. P. Luschen, Mark H. Fischer, Ronen Vosk, Ehud Altman, Ulrich Schneider, and Immanuel Bloch. Observation of many-body localization of interacting fermions in a quasirandom optical lattice. *Science*, 349(6250):842–845, 2015.

Norbert Schuch, Michael M Wolf, Frank Verstraete, and J Ignacio Cirac. Entropy Scaling and Simulability by Matrix Product States. *Physical Review Letters*, 100(3):030504, 2008.

Maksym Serbyn, Z. Papić, and Dmitry A. Abanin. Local Conservation Laws and the Structure of the Many-Body Localized States. *Physical Review Letters*, 111(12):127201, 2013.

Mark Srednicki. Chaos and quantum thermalization. *Physical Review E*, 50 (2):888–901, 1994.

Mark Srednicki. The approach to thermal equilibrium in quantized chaotic systems. *Journal of Physics A: Mathematical and General*, 32(7):1163–1175, 1999.

Marco Távora, E. J. Torres-Herrera, and Lea F. Santos. Inevitable Power-law Behavior of Isolated Many-Body Quantum Systems and How It Anticipates Thermalization. *Physical Review A*, 94(4):1–5, 2016.

E. J. Torres-Herrera and Lea F. Santos. Dynamics at the many-body localization transition. *Physical Review B*, 92(1):014208, 2015.

Matthias Troyer and Uwe-Jens Wiese. Computational Complexity and Fundamental Limitations to Fermionic Quantum Monte Carlo Simulations. *Physical Review Letters*, 94(17):170201, 2005.

C. J. Turner, A. A. Michailidis, D. A. Abanin, M. Serbyn, and Z. Papić. Quantum scarred eigenstates in a Rydberg atom chain: entanglement, breakdown of thermalization, and stability to perturbations. *Physical Review B*, 94(15):1–25, 2018a.

C. J. Turner, A. A. Michailidis, D. A. Abanin, M. Serbyn, and Z. Papić. Weak ergodicity breaking from quantum many-body scars. *Nature Physics*, 14 (7):745–749, 2018b.

Merlijn van Horssen, Emanuele Levi, and Juan P. Garrahan. Dynamics of many-body localization in a translation-invariant quantum glass model. *Physical Review B*, 92(10):100305, 2015.

F Verstraete and J. Ignacio Cirac. Renormalization algorithms for Quantum-Many Body Systems in two and higher dimensions. pages 1–5, 2004.

F Verstraete and J. Ignacio Cirac. Matrix product states represent ground states faithfully. *Physical Review B*, 73(9):094423, 2006.

F. Verstraete, J. J. Garcia-Ripoll, and J. I. Cirac. Matrix Product Density Operators: Simulation of finite-T and dissipative systems. *Physical Review Letters*, 93(20):1–5, 2004a.

F Verstraete, D Porras, and J. Ignacio Cirac. Density Matrix Renormalization Group and Periodic Boundary Conditions: A Quantum Information Perspective. *Physical Review Letters*, 93(22):227205, 2004b.

Guifré Vidal. Efficient Simulation of One-Dimensional Quantum Many-Body Systems. *Physical Review Letters*, 93(4):040502, 2004.

Alexander Weiße, Gerhard Wellein, Andreas Alvermann, and Holger Fehske. The kernel polynomial method. *Reviews of Modern Physics*, 78(1):275–306, 2006.

Steven R White. Density matrix formulation for quantum renormalization groups. *Physical Review Letters*, 69(19):2863–2866, 1992.

Steven R White. Density-matrix algorithms for quantum renormalization groups. *Physical Review B*, 48(14):10345–10356, 1993.

F. Alexander Wolf, Jorge A. Justiniano, Ian P. McCulloch, and Ulrich Schollwöck. Spectral functions and time evolution from the Chebyshev recursion. *Physical Review B*, 91(11):115144, 2015.

Michael M Wolf, Frank Verstraete, Matthew B Hastings, and J. Ignacio Cirac. Area Laws in Quantum Systems: Mutual Information and Correlations. *Physical Review Letters*, 100(7):070502, 2008.

H. D. Xie, R. Z. Huang, X. J. Han, X. Yan, H. H. Zhao, Z. Y. Xie, H. J. Liao, and T. Xiang. Reorthonormalization of Chebyshev matrix product

states for dynamical correlation functions. *Physical Review B*, 97(7):1–9, 2017.

Yilun Yang, Sofyan Iblisdir, J. Ignacio Cirac, and Mari Carmen Bañuls. Probing Thermalization through Spectral Analysis with Matrix Product Operators. *Physical Review Letters*, 124(10):100602, 2020.

# Acknowledgements

I would like to first thank my supervisor Ignacio Cirac for offering me the opportunity to do research in his excellent group as well as for his guidance to this project. His insights and passion in physics inspire me greatly. I am looking forward to continuing my PhD study under his supervision.

Second, I would like to express special gratitude to my co-supervisor Mari Carmen Bañuls. I benefit a lot from our discussions, especially regarding implementations of numerical methods. Her patience and encouragement were major factors for the success of this work. Thanks to my collaborator Sofyan Iblisdir as well for his valuable ideas.

I am also grateful to all members of the MPQ theory group and all TMP fellow students for the good moments spent together. And many thanks to my friends in Munich who have accompanied me during my Master study.

Last but not least, I would like to say the deepest thank to my family, for their love and unconditional support.

# Declaration of Authorship

I hereby declare that this thesis has been composed by myself and is based entirely on my work unless where clearly stated otherwise.

Yilun Yang

_____

Signature, city, date